



Since January 2020 Elsevier has created a COVID-19 resource centre with free information in English and Mandarin on the novel coronavirus COVID-19. The COVID-19 resource centre is hosted on Elsevier Connect, the company's public news and information website.

Elsevier hereby grants permission to make all its COVID-19-related research that is available on the COVID-19 resource centre - including this research content - immediately available in PubMed Central and other publicly funded repositories, such as the WHO COVID database with rights for unrestricted research re-use and analyses in any form or by any means with acknowledgement of the original source. These permissions are granted for free by Elsevier for as long as the COVID-19 resource centre remains active.



Carbon fullerene and nanotube are probable binders to multiple targets of SARS-CoV-2: Insights from computational modeling and molecular dynamic simulation studies

Sinosh Skariyachan^{a,*}, Dharshini Gopal^{b,c,1}, Dhrithi Deshpande^d, Anusha Joshi^e, Akshay Uttarkar^f, Vidya Niranjan^f

^a Department of Microbiology, St. Pius X College, Rajapuram, Kasaragod, Kerala, India

^b Faculté de Médecine et Pharmacie, Université Grenoble Alpes, Grenoble, France

^c Department of Bioinformatics, Manipal School of Life Sciences, Manipal Academy of Higher Education, Manipal, India

^d Department of Pharmacology and Pharmaceutical Sciences, School of Pharmacy, University of Southern California, Los Angeles, California, USA

^e Department of Molecular Cell Biology, University of Bonn, Bonn, Germany

^f Department of Biotechnology, RV College of Engineering, Bengaluru, Karnataka, India

ARTICLE INFO

Keywords:

Carbon nano fullerene
Carbon nanotube
COVID-19
Molecular docking
Molecular dynamic simulation

ABSTRACT

The present study aimed to predict the binding potential of carbon nanotube and nano fullerene towards multiple targets of SARS-CoV-2. Based on the virulent functions, the spike glycoprotein, RNA-dependent RNA polymerase, main protease, papain-like protease, and RNA binding domain of the nucleocapsid proteins of SARS-CoV-2 were prioritized as the molecular targets and their three-dimensional (3D) structures were retrieved from the Protein Data Bank. The 3D structures of carbon nanotubes and nano-fullerene were computationally modeled, and the binding potential of these nanoparticles to the selected molecular targets was predicted by molecular docking and molecular dynamic (MD) simulations. The drug-likeness and pharmacokinetic features of the lead molecules were computationally predicted. The current study suggested that carbon fullerene and nanotube demonstrated significant binding towards the prioritized multi-targets of SARS-CoV-2. Interestingly, carbon nanotube showed better interaction with these targets when compared to carbon fullerene. MD simulation studies clearly showed that the interaction of nanoparticles and selected targets possessed stability and conformational changes. This study revealed that carbon nanotubes and fullerene are probably used as effectual binders to multiple targets of SARS-CoV-2, and the study offers insights into the experimental validation and highlights the relevance of utilizing carbon nanomaterials as a therapeutic remedy against COVID-19.

1. Introduction

The outrageous outbreak of COVID-19 caused by Severe Acute Respiratory Syndrome Coronavirus-2 (SARS-CoV-2) which emerged in December 2019 in China spread worldwide (Ali and Alharbi, 2020; Han et al., 2021). The World Health Organization (WHO) declared coronavirus a pandemic on March 11, 2020 (World Health Organization, 2020). Organizations globally debated and discussed potential therapeutic strategies for treating COVID-19 as the world has been witnessed the second wave of coronavirus which is much more life-threatening than what was observed during the first outbreak. It has currently resulted in 25.2Cr confirmed infected cases and 50.8 L deaths across the

world as of 12 November 2021 according to the statistics of WHO (World Health Organization, 2021). The infection rate of COVID-19 is high, its incubation period is long and with its symptoms being mild to moderate, this disease is highly troubling. This global pandemic has changed the lifestyle of people across the globe affecting the economic, business, food, education, research sectors along with the health sector (Naserghandi et al., 2020). Countries such as India are in excruciating threat as medical resources cannot meet the needs of the entire population and due to this particular reason, there has been an enormous spike in the number of infections and deaths nationwide.

Initially, flu-like symptoms occurred after 3–14 days of exposure to SARS-CoV-2 in healthy individuals and severe pneumonia in

* Corresponding author at: Department of Microbiology, St. Pius X College, Rajapuram, Kasaragod, Kerala, India.

E-mail address: sinoshmicro@stpius.ac.in (S. Skariyachan).

¹ Joined the first author, equally contributed.

<https://doi.org/10.1016/j.meegid.2021.105155>

Received 29 September 2021; Received in revised form 12 November 2021; Accepted 18 November 2021

Available online 22 November 2021

1567-1348/© 2021 The Authors.

Published by Elsevier B.V. This is an open access article under the CC BY-NC-ND license

(<http://creativecommons.org/licenses/by-nc-nd/4.0/>).

immunocompromised patients (Kannan et al., 2020). However, there are several reports with various ranges of symptoms that have resulted in the COVID-19 infection. Apart from the reported symptoms, a major group of asymptomatic individuals tested positive for the infection even without showing symptoms (Palacios Cruz et al., 2020). SARS-CoV-2 belongs to a group of viruses known as coronaviruses which are positive-stranded RNA viruses belonging to the β -coronaviruses family (Cascella et al., 2021), they have a crown-like appearance because of the presence of spike glycoproteins on the envelope. Other main structural proteins of SARS-CoV-2 include nucleocapsid protein, membrane protein, envelope protein, nucleocapsid protein, and RNA depending on RNA polymerase (Srinivasan et al., 2020; Dai and Gao, 2021).

Initially, the treatment suggested for COVID-19 infection includes the administration of antivirals such as lopinavir, ritonavir, remdesivir, chloroquine, and hydroxychloroquine (Rahimi and Abadi, 2020). However, a recent review suggested that chloroquine and hydroxychloroquine are not effective against COVID-19 (Altulea et al., 2021). Several vaccines/drugs are at the clinically developmental stages, and it is one of the most challenging tasks as a pandemic like this has never been witnessed previously (Rahimi and Abadi, 2020). The precise and rapid tracking of the genetic changes of SARS-CoV-2 facilitates faster clinical tests and predicts the efficiency of the vaccines. As sequencing technologies and genomic analysis tools progress, genome sequencing is becoming more widely integrated into clinical and healthcare workflows. Utilizing these technologies, several new variants have been identified in different parts of the world. Recent studies suggested that there were several mutational variants such as B.1.1.7 (alpha), B.1.351 (beta), B.1.1.28.1 (gamma or p.1), (delta), and B.1.617.2 B.1.617.1 (kappa) identified in the spike protein. These variants showed increased transmission and virulence and decreased neutralization (Krause et al., 2021). Currently, vaccines are available to treat COVID-19, however, the vaccines have not yet reached the communities in several countries, where 99.5% of the patients who died over the past several months were found to be unvaccinated. The diverse symptoms observed in the patients and asymptomatic transmission, the aforementioned vaccine-resistant data shows that making the development of an alternative therapeutic solution/drug emergently essential as well as critically challenging (Shin et al., 2020; Yüce et al., 2021).

As the conventional methods of drug development are extremely time-consuming and require expensive infrastructure, computational biology aids in this process by contributing to a faster and cost-effective approach (Melanthota et al., 2020; Skariyachan et al., 2020). With the recent advancement in nanotechnology, carbon nanoparticles such as carbon nano fullerene and nanotube could be employed for targeting multiple targets of SARS-CoV-2 and inhibiting their virulent functions (Starsich et al., 2019). Carbon nanotubes (CNTs) are reported to be the new materials with therapeutic properties due to their exceptional mechanical features, functional group modifiability, and structural stability. (Shirasu et al., 2021). A recent review suggested that nanomaterials can be used to develop novel biocompatible nano-based materials for drug/vaccine delivery systems against COVID-19 (Tang et al., 2021). Nanomaterials are useful in developing nano-based protection equipment and disinfecting agents against COVID-19 (Singh et al., 2021). The non-toxic antiviral NPs are currently under development for clinical application to treat COVID-19 (Tavakol et al., 2021). Further, NPs can be used as a carrier for antigens or as an adjuvant, and design new generation vaccines against COVID-19 (Rai et al., 2021). As carbon nanoparticles are known for their inhibitory properties against various microorganisms, it would be essential to learn about their binding and inhibitory potential against SARS-CoV-2 targets (Bhavana et al., 2020). An interesting association between cancer and COVID-19 was illustrated to make it emergently effective for immunocompromised patients proposing the use of nanotechnology for vaccine development (Walls et al., 2020). Similarly, silicon nanowire sensors are promising devices to detect viruses and proteins (Mirsian et al., 2019). The nanowire field-effect troponin sensors are used to detect prostate cancer and

myocardial infarction (Khodadadian et al., 2017).

The present study combines computational biology and nanotechnology to predict and understand the molecular and atomic interactions between the carbon nanoparticles and putative targets of SARS-CoV-2 by performing molecular docking and molecular dynamic simulations. The current study aimed to predict the binding potential of carbon nano fullerene and nanotubes to multiple potential targets of SARS-CoV-2 by computational virtual screening and molecular dynamic simulation studies. The study initially focused to screen the three-dimensional structures of five major targets of SARS-CoV-2 and predict the binding potential of both carbon nano fullerene and nanotube towards multiple targets by molecular docking. The stability of the best interaction complexes of the carbon fullerene and nanotubes with the selected protein targets were further evaluated by molecular dynamic simulation studies and the study prioritized the application of carbon-based nanomaterial as putative lead molecules against the multiple targets of SARS-CoV-2.

2. Results and discussion

Though vaccines are available to some extent to challenge COVID-19, the second wave of the disease by several variants of SARS-CoV-2 caused a high rate of mortality and morbidity every day, and the issues have become a prime concern worldwide. In the absence of drugs, the identification of potential therapeutic lead molecules has scope and applications. Computational biology and high throughput screening provide a significant role in identifying potential molecular targets, screening and scrutinizing lead candidates with ideal drug-likeness, pharmacokinetics, and toxicities, and providing scope and application in drug discovery. It is known that nanomaterials have significant applications in medicinal chemistry, and they are widely used as drug delivery systems. Further, several nanomaterials have effectual binding to several molecular targets, and their application as a potential binder against multi-targets of SARS-CoV-2 has not yet been adequately explored. Thus, the study is aimed to predict the binding potential of carbon nanotube and nano fullerene, two important nanoparticles with well-known medical applications, towards multiple targets of SARS-CoV-2. It is expected that the outcome of this study offers profound insights into the experimental validation and highlights the relevance of utilizing carbon nanomaterials as a therapeutic remedy against COVID-19.

2.1. Identification of putative targets and their structural features

Based on an extensive literature survey and virulent features of the pathogen, five prominent targets (Fig. 1) of SARS-CoV-2 were identified as shown in Table 1. Spike glycoprotein (PDB ID: 6VSB) is involved in promoting the entry through the transmembrane spike into cells and is the main target of antibodies. The transmembrane spike consists of two functional subunits responsible for binding to the host cell receptors and fusion of the viral and cellular membrane. Depending on the viral strain, different viruses use different domains within the host cell receptor subunit to recognize various points of attachment and entry (Romeo et al., 2020). The RNA-dependent RNA polymerase (RdRp) (PDB ID: 6M71) is the main component responsible for the replication and transcription of the viral (corona-viral) machinery and is essential for the survival of these viruses (Gao et al., 2021). The active site of RdRp is conserved and accessible, therefore targeting this region would be an ideal approach (Aftab et al., 2020; Yin et al., 2020). The main protease is an enzyme that also plays a crucial role in viral replication and transcription (Dai et al., 2020). Along with papain-like protease (which is also a deubiquitinase), the main protease is essential for processing the polyproteins that are translated from the viral RNA. Inhibition of these proteases would help in blocking viral replication (Zhang et al., 2020). The main protease exclusively cleaves the polypeptide sequences following a glutamine residue, making it an ideal drug target, as

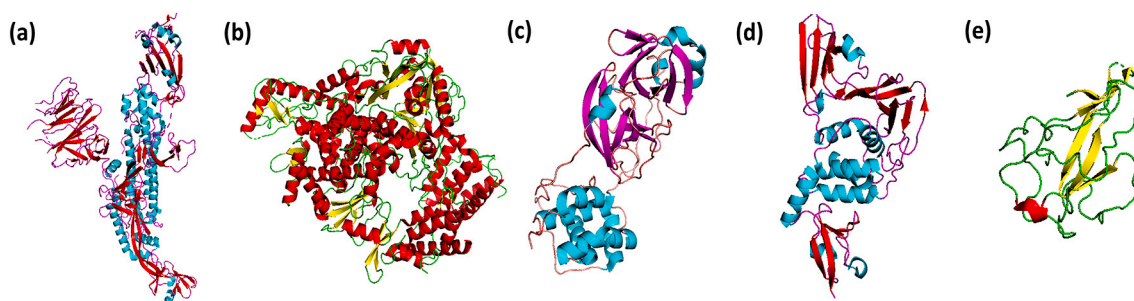


Fig. 1. The potential drug targets of SARS-CoV-2 selected in the present study (a) Spike glycoprotein, (b) RNA directed RNA polymerase, (c), Main protease, (d) Papain-like protease and (e) RNA binding domain of Nucleocapsid protein.

Table 1

Putative targets of SARS-CoV-2 identified based on pathogenic function.

Protein target name	Function	Structural information			References
		PDB ID	Experiment used	Resolution	
Spike glycoprotein	Mediates host transfer and counteracts the antiviral activity of the host protein	6VSB	Cryo-electron microscopy	3.46 Å	Wrapp et al., 2020
RNA dependent RNA polymerase	Responsible for the replication and transcription of the viral RNA	6M71	Electron microscopy	2.90 Å	Gao et al., 2020
Main protease	Responsible for the cleavage of C terminus of the polyprotein	6LU7	X-ray diffraction	2.16 Å	Jin et al., 2020
Papain-like protease	Responsible for the cleavage of the N terminus of the polyprotein into functional products	6W9C	X-ray diffraction	2.70 Å	Osipiuk et al., 2020
RNA binding domain of Nucleocapsid protein	Plays a fundamental role in enhancing the efficiency of sub genomic viral transcription and replication	6M3M	X-ray diffraction	2.70 Å	Kang et al., 2020

according to Ullrich et al., no human host-cell proteases are known with this substrate specificity (Ullrich and Nitsche, 2020). The disease can be attenuated by inhibition which impedes the production of infectious viral particles. Papain-like protease also plays a vital role in virus replication and immune evasion, similar to the main-protease. The structures of SARS-CoV and SARS-CoV-2 papain-like protease domains share almost indistinguishable structural features and inhibitors developed for SARS-CoV could be found to be effective for SARS-CoV-2 (Gao et al., 2020a). The RNA binding domain of the nucleocapsid protein plays a significant role in regulating viral RNA synthesis in replication and transcription, and in modulating the infected cell metabolism (Kang et al., 2020). The nucleocapsid protein is conserved, more stable, and is

immunogenic in many coronaviruses, and is expressed abundantly during infection (Cong et al., 2020; Dutta et al., 2020). Thus, these proteins were selected for the current study as they could be possible putative drug targets for the SARS-CoV-2 infection.

2.2. Pharmacokinetic features of carbon nanoparticles

The retrieved and modeled chemical structures of the carbon nanoparticles (Fig. 2) were used for the drug-likeness, ADME and toxicity features prediction, and the obtained results are shown in Table 2. Both carbon nano fullerene and nanotube show the same drug-likeness properties according to the predictions of the PreADMET tool. All the

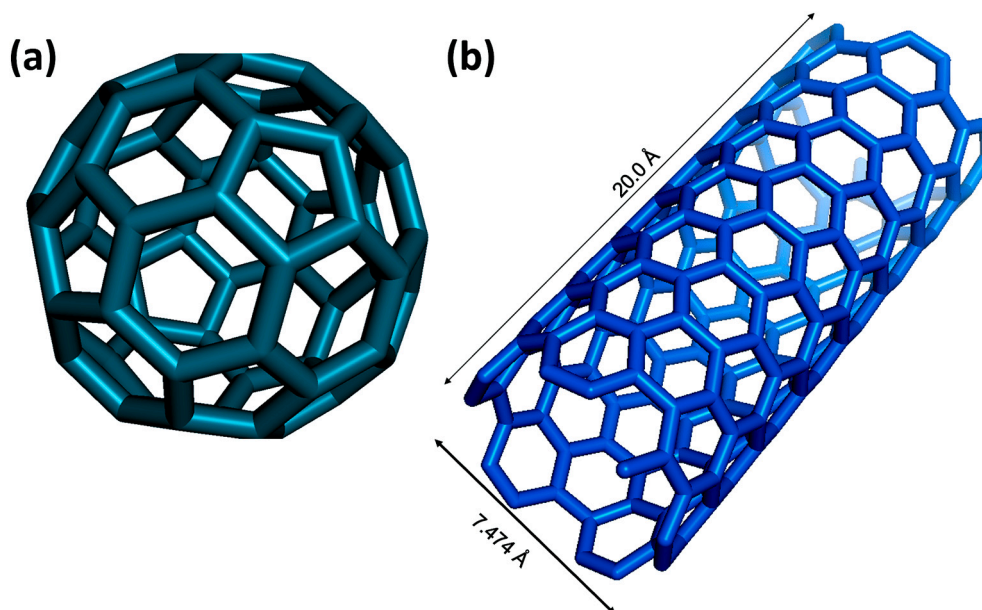


Fig. 2. The structure of the nanomaterials used in the current study (a) Carbon nano fullerene and (b) carbon nanotube.

Table 2

Druglikeness and Pharmacokinetic features of carbon nano fullerene and carbon nanotube predicted using PreADMET and admetSAR.

Name of the particles		Carbon nano fullerene	Carbon nanotube (6, 5)	
Drug likeness	CMC like rule	Not qualified	Not qualified	
	Lead like rule	Violated	Violated	
	MDDR like rule	Mid-Structure	Mid-Structure	
	Rule of Five	Violated	Violated	
	WDI like rule	Out of 90% cut off	Out of 90% cut off	
ADME	Blood-Brain Barrier	28.2401	31.3645	
	CaCo-2 (nm/s)	22.1611	23.2743	
	Human Intestinal Absorption (%)	100.0000	96.1654	
	Plasma Protein Binding (%)	100.0000	100.0000	
	Skin Permeability (cm/h)	-5.0254	-5.0309	
	Human oral bioavailability	Positive	Positive	
	Toxicity	Ames test	Mutagen	Mutagen
Carcinogen test		Mouse	Positive	Positive
		Rat	Negative	Negative
hERG inhibition		Medium risk	Medium risk	
Daphnia test		2.62308e-006	7.81067e-018	
Fish toxicity		Medaka	3.8803e-010	6.97767e-030
		Minnow	3.89314e-008	1.21979e-022
Algae test		0.0017	2.57772e-098	
Hepatotoxicity (%)		72.50	70.00	
Honey bee toxicity (%)		71.75	73.42	
Eye corrosion (%)		58.00	60.00	
Eye irritation (%)		98.19	96.22	

molecular descriptors of drug-likeness are predicted to be violated by these nanoparticles. They did not qualify CMC-like rule, violated the Lead-like rule and rule of five, mid-structural (between a drug and lead molecule) property was obtained by the MDDR report and they were out of 90% cut-off as predicted by the WDI index. However, most of the currently used conventional drugs do not qualify all the descriptors of drug-likeness predictions and result in similar predictions as obtained for the nanoparticles employed in our study.

The ADME predictions of the carbon nanoparticles obtained by PreADMET and admetSAR are given in Table 2. Blood-brain barrier, logBB ($\log[\text{brain}]/[\text{blood}]$) was predicted to be 28.2401 and 31.3645 for fullerene and nanotube respectively. These values predicted are within the acceptable range of the statistical models. The human epithelial colorectal adenocarcinoma cell (caco-2) permeability was predicted to be 22.16 and 23.27 nm/s. The human intestinal absorption was found to be 100% and 96%, respectively implying good absorption. Similarly, the plasma protein binding was predicted to be 100% for both nanoparticles. Skin permeability was predicted to be -5 cm/h for both the nanoparticles. Finally, the oral bioavailability was found to be positive. These properties make the nanoparticles suitable for applications in the biomedical field.

Despite all the marvelous and expanding applications of nanoparticles in the field of therapeutics, toxicity has been questioned for years now. Predictions obtained from PreADMET and admetSAR are shown in Table 2. The mutagenicity using the Ames test model predicted that both the particles are possible mutagens. Carcinogenicity in the mouse and rat models was predicted to be positive and negative, respectively for both the nanoparticles. It is noteworthy that they are known for their remarkable applications in cancer therapy. The human ERG inhibition was predicted to exhibit medium risk. Hepatotoxicity was predicted to be around 70%, eye irritation was >95% and eye corrosion was ~60% toxic. Daphnia, algae, honey bee, minnow, and medaka fish toxicities of the nanoparticles were mild according to the predictions obtained.

In recent years, several studies have been reported indicating that nanoparticles can be used for the treatment, and compared to other

drugs, there is greater bioavailability and stable release of drugs using carbon nanoparticles (Zhao et al., 2020). Nanoparticles have been used previously as drug delivery agents to targeted tissues and cells. These nanoparticles can be coated with different compounds and functionalization of these compounds reduces systemic toxicity and improves the efficacy of drugs. Some verified studies also indicate that carbon nanotubes can be used as delivery systems for genes, antigens, etc. across cell lines with almost negligible toxicity (Saleemi et al., 2020). As the predicted results are similar to those of currently prescribed drugs, nanoparticles could be employed for the treatment of COVID-19 infection.

2.3. Molecular docking

AutoDock vina (Trott and Olson, 2010) was used for docking the nanoparticles against the identified SARS-CoV-2 targets, and interactions of the docked complexes were analyzed. The obtained binding energy (kcal/mol), root mean square deviation (RMSD), and the number of hydrogen bonds and residues of the targets interacting with the nanoparticles are shown in Table 3 and depicted in Figs. 3 & 4 by visualizing on Maestro (Schrödinger Release 2020–4, 2020).

Carbon nano fullerene, also known as buckminsterfullerene (C60) exhibited promising binding affinity towards SARS-CoV-2 targets. It showed a binding affinity of -13.7, -12.9, -11.4, -10.6, and -10.1 kcal/mol towards spike glycoprotein, RNA dependent RNA polymerase, main protease, papain-like protease, and RNA binding domain of nucleocapsid protein, respectively. The amino acid residues of spike glycoprotein (PDB ID: 6VSB) interacting with fullerene include Tyr380, Pro412, Pro987, and Val991 as shown in Fig. 3a. These residues are present at the binding sites of the protein as predicted by CastP and Depth servers. RNA-dependent RNA polymerase (PDB ID: 6M71) - carbon nano fullerene docked complex shows interactions of fullerene with the residues Pro323, Pro461, Leu460, and Pro677 as shown in Fig. 3b. These interacting residues are present at the helix and beta-strand regions of the target and therefore, this interaction could suppress the function of the protein. The interacting residue of the main protease (PDB ID: 6LU7) includes Phe223 as shown in Fig. 3c. Ala39 and Ile44 present at the active sites of papain-like protease (PDB ID: 6W9C) interact with fullerene in the docked complex as depicted in Fig. 3d. The interacting residues of the RNA binding domain of nucleocapsid protein (PDB ID: 6M3M) include Ile75, Pro81, and Pro163 as shown in Fig. 3e. These residues are involved in binding at the phosphate groups of RNA of the virus which makes it an essential and promising interaction to inhibit the target.

Carbon nanotube (C182), modeled with 6, 5 chirality docked against the SARS-CoV-2 targets showed potential interactions that could inhibit the pathogenic mechanism of the virus. The binding energies of -26.7, -19.7, -15.8, -21.1, and -20.7 kcal/mol were exhibited towards spike glycoprotein, RNA dependent RNA polymerase, main protease, papain-like protease, and RNA binding domain of nucleocapsid protein, respectively. Interactions observed between the spike protein (PDB ID: 6VSB) and nanotube involved residues such Leu303, Lys310, Tyr313, Asp663, Arg765, Thr768, Val772, Lys776, Gly946, Asp950, and Asn953 as shown in Fig. 4a. These residues form a prominent part of structural integrity and this interaction could alter the structure thereby suppressing the pathogenic function of the spike protein. Interacting residues of RNA-dependent RNA polymerase (PDB ID: 6M71) include Phe35, Ile37, Lys41, Lys50, Lys73, Asp208, Asp218, and Asn713 as depicted in Fig. 4b. These residues are present at the binding sites of the protein as predicted by CastP and Depth servers. Asp245, Ile249, Pro252, Phe294, and Val297 are the residues of main protease (PDB ID: 6LU7) interacting with the nanotube as shown in Fig. 4c. These residues are present near the binding sites of Lopinavir and Ritonavir (Nutho et al., 2020), but with better binding energy could provide better results than the conventional antiviral drugs employed. The interacting residues of papain-like protease (PDB ID: 6W9C) are Leu36, Ala39, Ile44, Thr74, Thr75, Asp76, Lys92, Asn156, Gln174, and His175 shown in

Table 3

Binding energy and interactions between the targets and nanoparticles obtained from docking on AutoDock Vina.

Protein name	PDB ID	Ligand	Binding affinity (Kcal/mol)	RMSD (Å)	Interacting residues	Hydrogen bonds
Spike glycoprotein	6VSB	Fullerene	-13.7	0.0	Tyr380, Pro412, Pro987, Val991	-
		Nano tube	-26.7	0.0	Leu303, Lys310, Tyr313, Asp663, Arg765, Thr768, Val772, Lys776, Gly946, Asp950, Asn953	-
RNA dependent RNA polymerase	6M71	Fullerene	-12.9	0.0	Pro323, Leu460, Pro461, Pro677	-
		Nano tube	-19.7	0.0	Phe35, Ile37, Lys41, Lys50, Lys73, Asp208, Asp218, Asn713	-
Main protease	6LU7	Fullerene	-11.4	0.0	Phe223	-
		Nano tube	-15.8	0.0	Asp245, Ile249, Pro252, Phe294, Val297	-
Papain-like protease	6W9C	Fullerene	-10.6	0.0	Ala39, Ile44	-
		Nano tube	-21.1	0.0	Leu36, Ala39, Ile44, Thr74, Thr75, Asp76, Lys92, Asn156, Gln174, His175	-
RNA binding domain of Nucleocapsid protein	6M3M	Fullerene	-10.1	0.0	Ile75, Pro81, Pro163	-
		Nano tube	-20.7	0.0	Ala51, Ala91, Arg93, Arg150, Pro152, Tyr173, Ala174	-

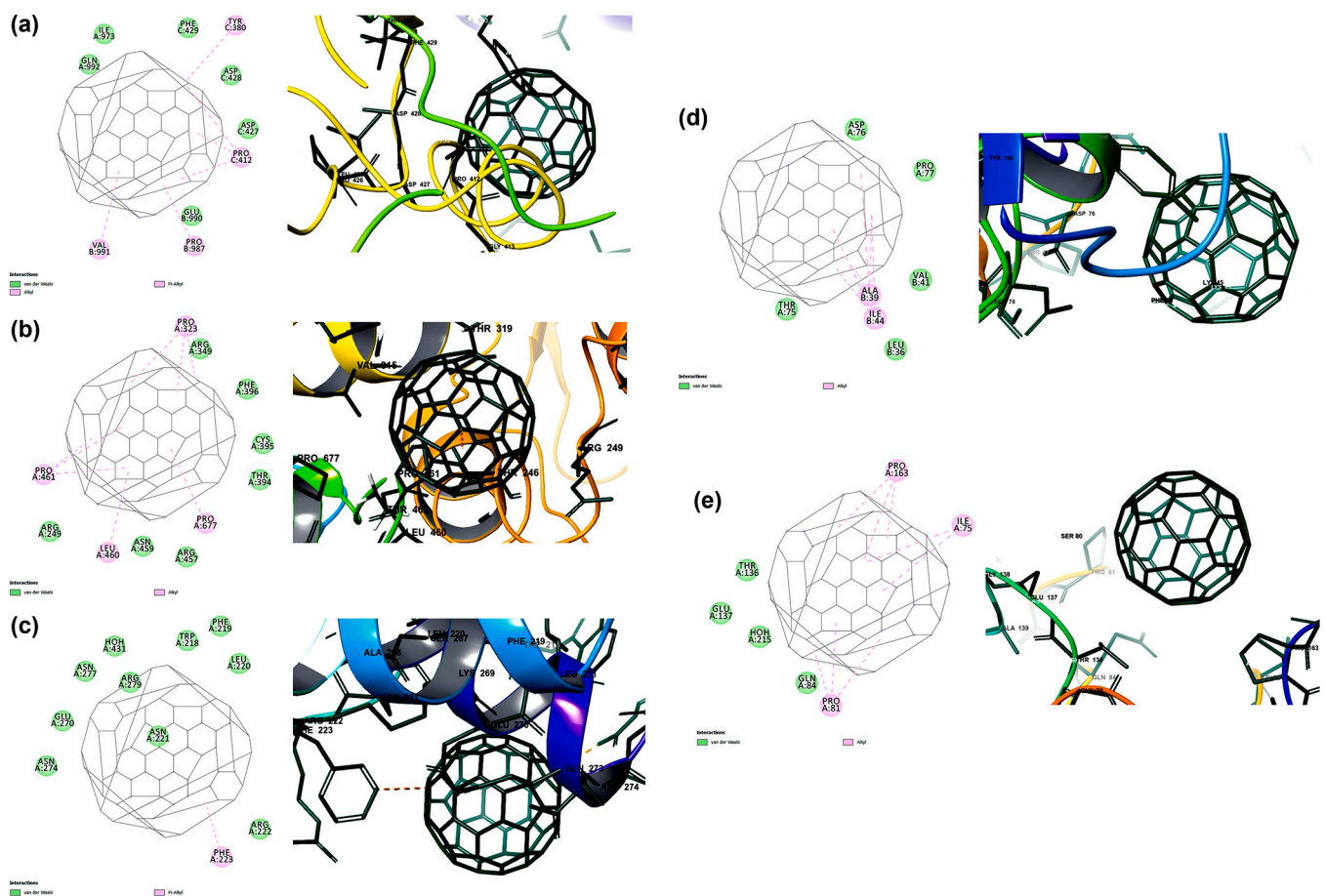


Fig. 3. The binding potential of carbon nanofullerene towards the prioritized targets of SARS-CoV-2 is predicted by molecular docking. The binding affinity and interactions of carbon nano fullerene towards (a) spike glycoprotein (-13.7 kcal/mol), (b) RNA dependent RNA polymerase (-12.9 kcal/mol), (c) main protease (-11.4 kcal/mol), (d) papain-like protease (-10.6 kcal/mol) and (d) RNA binding domain of nucleocapsid protein (-10.1 kcal/mol).

Fig. 4d. The residues Thr74, Gln174, and His175 are known to interact with conventional antiviral drugs such as nelfinavir and remdesivir (Mothay and Ramesh, 2020). Similarly, the residues of the RNA binding domain of nucleocapsid protein (PDB ID: 6M3M) interacting with carbon nanotube include Ala51, Ala91, Arg93, Arg150, Pro152, Tyr173, and Ala174 as shown in Fig. 4e. The residues involved in these docked interactions are essential to be targeted to inhibit the function of the virus.

2.4. Molecular dynamic simulation

The best binding poses of the SWCNT and nano-fullerene with the five selected targets predicted by molecular docking studies were selected and simulated using the Desmond module of Schrödinger's suite, to interpret the stability and dynamics of the interaction between the nanoparticles and SARS-CoV-2 targets. The interaction stability was confirmed by analyzing the simulation trajectories such as the changes and fluctuations in protein RMSD and root mean square fluctuations

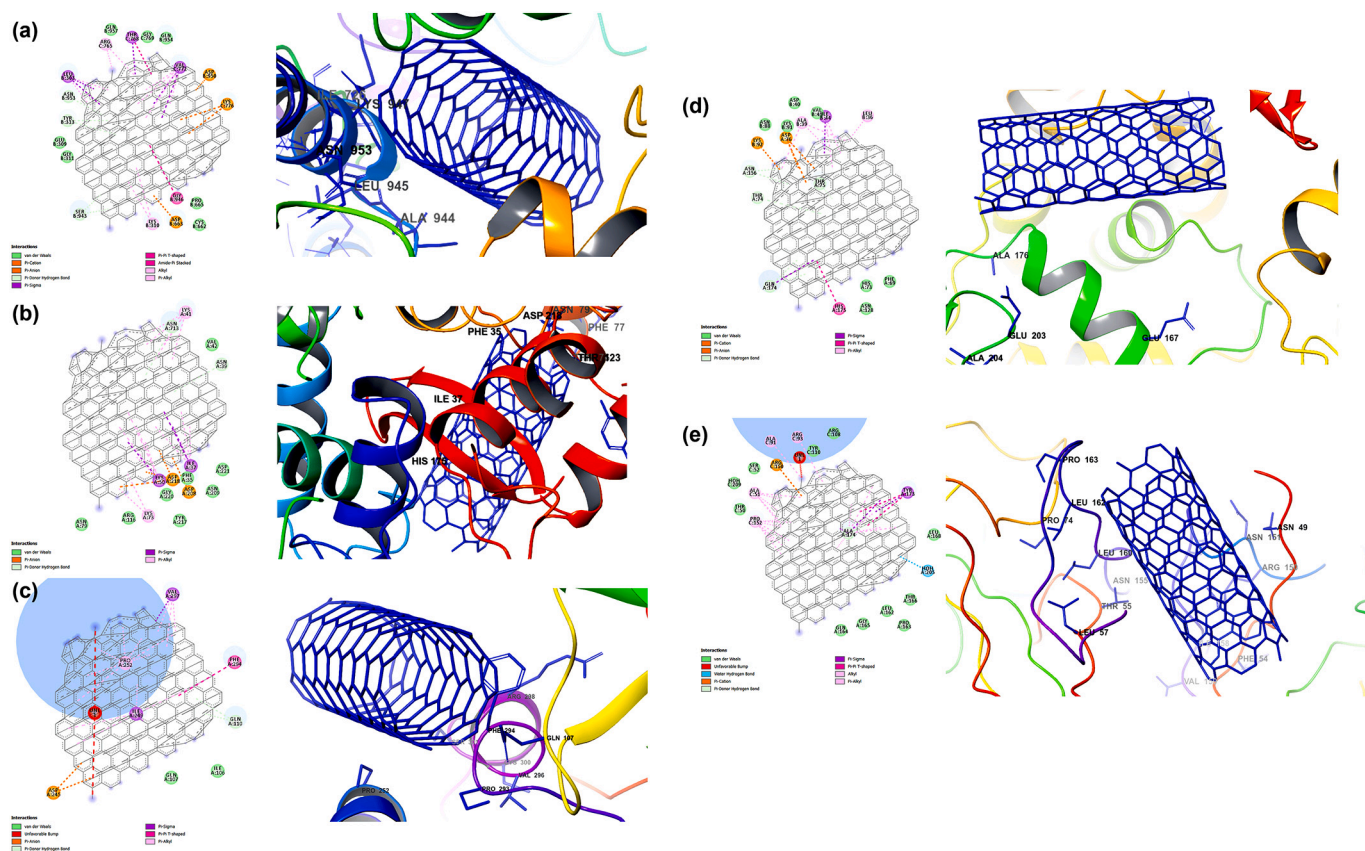


Fig. 4. The binding potential of carbon nanotube towards the prioritized targets of SARS-CoV-2 predicted by molecular docking. The binding affinity and interactions of carbon nanotube towards (a) spike glycoprotein (-26.7 kcal/mol), (b) RNA dependent RNA polymerase (-19.7 kcal/mol), (c) main protease (-15.8 kcal/mol), (d) papain - like protease (-21.1 kcal/mol) and (e) RNA binding domain of nucleocapsid protein (-20.7 kcal/mol).

(RMSF), ligand RMSF, interactions between the protein residues and ligands, changes occurring in the protein backbone, and ligand atoms throughout 100 ns. The trajectories obtained for spike glycoprotein (PDB ID: 6VSB) in complex with nano fullerene confirmed that the interactions exhibited on docking were stable. The protein RMSD, as shown in Fig. 5a, deviated between 3.1 and 5.6 Å throughout the simulation. The RMSD was below 4.0 Å, there on it increased stably and linearly up to 5.5 Å, as a result of the binding event that occurs between the nanoparticle and the macromolecule. Protein RMSF showed extremely high fluctuations ranging from 1.0 to >8.0 Å along the entire length of the receptor backbone, which represents the effect of the drug interaction with the target and is depicted in Fig. 5b. The interactions that occurred during the simulation are shown in Fig. 5c, to time. The top region represents total contacts that occurred throughout the simulation which is depicted to be an average of three to six interactions at any given point in time. From the bottom region, it can be observed that a total of ten residues constantly interacted with the ligand, out of which five residues such as Ile973, Pro987, Val991, Tyr380, and Phe429 showed were very prominent interactions. A histogram representing the interacting residues on the x-axis and interaction fraction on the y-axis is shown in Fig. 5d. From this complex, only hydrophobic interactions were observed, and five residues have an interaction fraction of >0.5 towards the ligand which confirms the stability of the complex interaction. Ligand RMSD fluctuation is shown in Fig. 5e, and it is observed to be >3.0 Å as the ligand atoms undergo significant changes during the interaction events. The interactions that occurred for greater than 10% of the simulation period are shown in Fig. 5f, and Ile973, Pro987, and Val991 were the residues involved in the hydrophobic interactions with carbon fullerene. The structural changes undergone by the target and ligand are shown in Supplementary figs. S1 & S2. The secondary

structural changes and helicity of the proteins and the conformational changes of secondary structural elements during the simulation indicated that the protein undergoes conformational flexibility during the interaction with the carbon nanoparticles. Overall, the docked complex and the interactions involved were observed to be stable in the applied dynamic conditions.

The RdRp (PDB ID: 6M71) and fullerene complex trajectories obtained from the MD simulation are given in Fig. 6. The RMSD of the receptor protein was observed to be stable till about 80 ns which was less than 3.0 Å, thereafter a sudden increase up to 9.0 Å is observed as shown in Fig. 6a. From 80 to 100 ns the RMSD fluctuates between 3.0 and 9.0 Å, which is high indicating the severe changes undergone by the protein as a result of interacting with fullerene. The RMSF of the receptor was also obtained with high fluctuations, that is, in the range of 0.8–6.5 Å as shown in Fig. 6b. These fluctuations imply that the ligand has a significant effect on suppressing the receptor thereby inhibiting its function. The interactions and the amino acids involved in the interaction are shown in two different panels to time in Fig. 6c. The top panel indicates the total number of interactions throughout the simulation course which on average is about 5, whereas the bottom panel represents the 15 residues interacting with fullerene to time, out of which 6 residues such as Arg249, Pro323, Phe396, Leu460, Pro461, and Pro677 interact constantly compared to the other amino acids. The interaction fraction of each of the interacting residues is depicted using a histogram in Fig. 6d. All the observed contacts are hydrophobic and the six aforementioned residues have >0.4 interaction involvement. The ligand RMSF is >3.5 Å as a result of the atoms being broken down during the binding event as shown in Fig. 6e. The binding that occurs for more than 10% of the simulation period is pictorially represented in Fig. 6f, and Trp268, Pro323, Leu460, Pro461, and Pro677 are the residues involved.

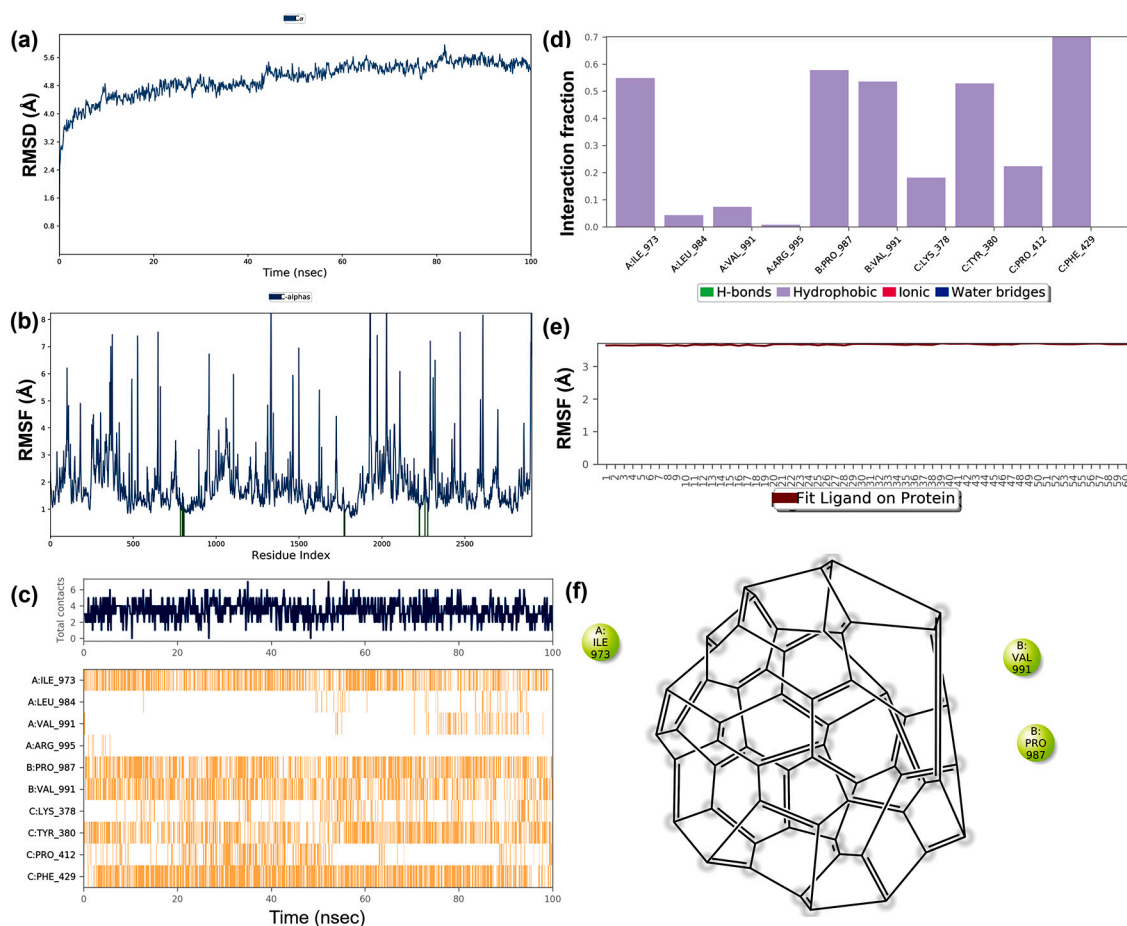


Fig. 5. The MD simulation trajectories of spike protein and nano fullerene complex (a) RMSD: Protein RMSD (Å) on the y-axis and time on the x-axis (b) Protein RMSF (Å) on the y-axis and residues on the x-axis (c) Protein-ligand contacts over the simulation course, (d) histogram representing interaction fraction on the y-axis and residues on the x-axis (e) Ligand RMSF (Å) on the y-axis and atoms on the x-axis and (f) Major interactions that occur during MD simulation.

The structural and chemical changes that the target and ligand undergo throughout 100 ns are shown in Supplementary figs. S3 & S4. Altogether, it is evident that the docked complex and the dynamic interactions involved are relatively stable.

The docked complex of the main protease (PDB ID: 6LU7) and fullerene, when simulated, produced trajectories that are shown in Fig. 7. The deviation in the protein RMSD was obtained to be between 1.2 and 3.6 Å as shown in Fig. 7a. The RMSD reached the highest peak around 45 ns to 3.6 Å, thereafter, for about 30 ns, it remained stable in the range of 2.2–2.8 Å, and it came back to 1.2 Å in the last 10 ns. These large variations are a result of the ligand binding to the protein backbone. The RMSF fluctuations in the protein backbone were observed to be as high as 5.4 Å in the C- and N- terminal regions, whereas, the rest of the protein structure had an RMSF of about 1.6 Å on average, as depicted in the plot of Fig. 7b. The bonds formed between the target and the nanoparticle; the residues involved in the bond formation are elucidated in Fig. 7c. The top region represents the number of interactions throughout the simulation which is about 2 at any given point of simulation time and the bottom region represents 7 residues that are involved in the interaction, out of which Trp218 is the most prominent one followed by Phe223, Leu271, and Arg279. A histogram showing that Trp218 has the highest interaction fraction of about 0.7, followed by Phe223 (0.5), Arg279 (0.4), and Leu271 (0.3) is given in Fig. 7d. The Ligand RMSF, in this case, was about 4.0 Å as the atoms break as and when they interact with the target molecule which is shown in Fig. 7e. The residues such as Phe223 and Leu271, that interact with the ligand for more than 10% of the simulation period are represented in Fig. 7f.

The changes that occur to the structures of protein and ligand are shown in Supplementary figs. S5 & S6. Overall, the docked complex interactions and energies are observed to be dynamically stable.

The simulation results obtained for the papain-like protease (PDB ID: 6W9C) and fullerene complex are shown in Fig. 8. The changes in the RMSD of the protein backbone are depicted in Fig. 8a, and it can be observed that it increases stably up to 60 ns and thereby stabilizes between 6.0 and 7.0 Å in the next 40 ns due to the fullerene interaction. The plot of protein RMSF which is given in Fig. 8b, shows very high fluctuations throughout the protein structure ranging from 1.0 to 7.0 Å, indicating the effect of fullerene on the receptor structure. The interaction plots are given in Fig. 8c, where the top panel represents the contacts and the bottom panel represents the 12 interacting amino acids to time. The prominent interactions involved the residues Leu36, Ile44 and Pro77. The fraction for the residue interaction was plotted using a histogram as shown in Fig. 8d. It can be observed that the aforementioned amino acids showed a 0.5–0.7 fraction of interaction supporting the previous statement. The ligand RMSF fluctuates between around 4.0 Å (Fig. 8e), as the atoms break down during the interaction to inhibit the protein structure. The interaction profile showing prominent interactions that occurs greater than 10% of the simulation time is shown in Fig. 8f. The changes that occur to the structures of protein and ligand are shown in Supplementary figs. S7 & S8. Overall, the docked complex interactions and energies are observed to be dynamically stable.

The RNA binding domain of the nucleocapsid protein structure in complex with fullerene, when simulated generated trajectories as shown in Fig. 9. The protein RMSD initially increased to about 9.0 Å, and there

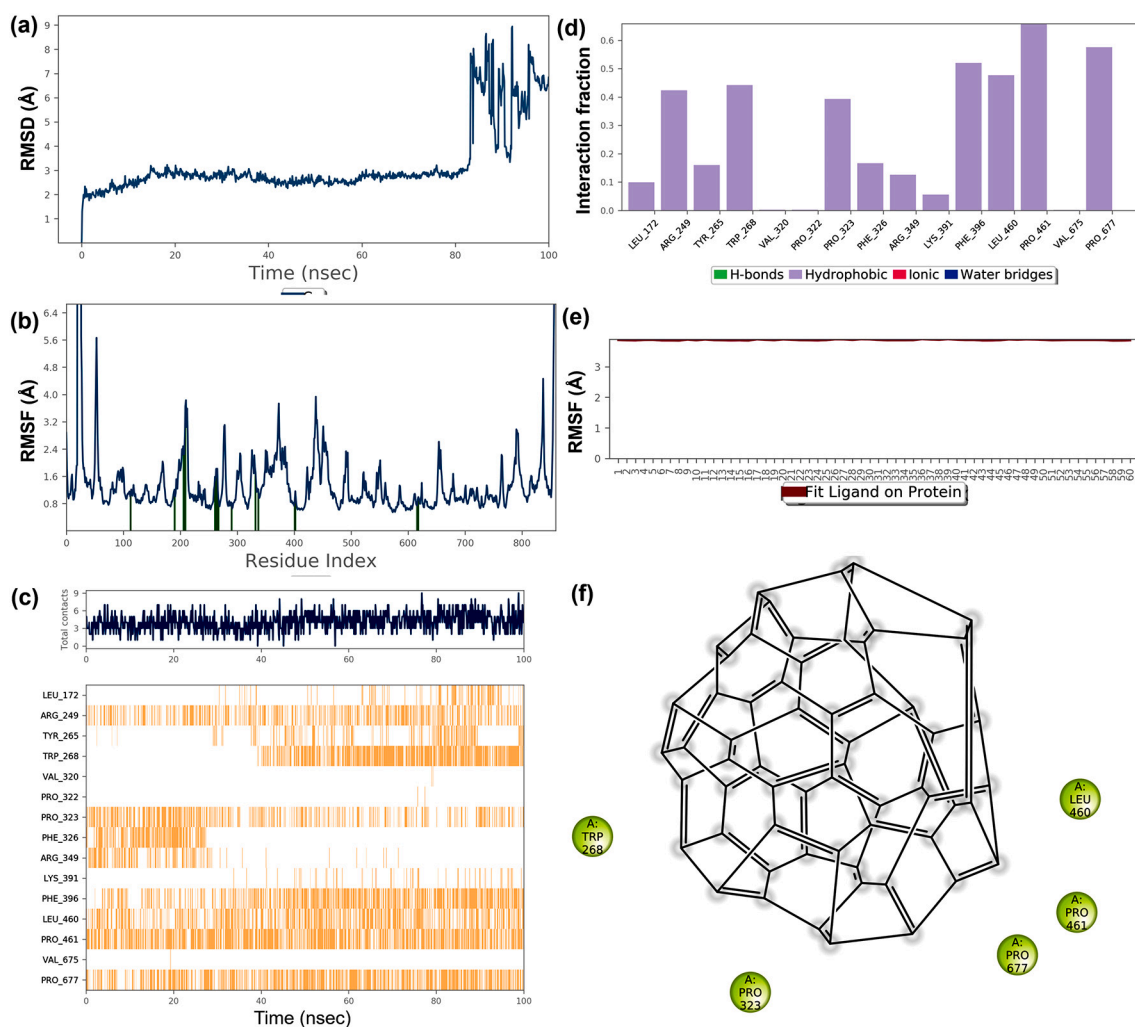


Fig. 6. The MD simulation trajectories of RdRp protein and nano fullerene complex (a) RMSD: Protein RMSD (Å) on the y-axis and time on the x-axis (b) Protein RMSF (Å) on the y-axis and residues on the x-axis (c) Protein-ligand contacts over the simulation course, (d) histogram representing interaction fraction on the y-axis and residues on the x-axis (e) Ligand RMSF (Å) on the y-axis and atoms on the x-axis and (f) Major interactions that occur during MD simulation.

on, remained stable with less than 0.5 Å deviation as shown in Fig. 9a. This high RMSD is obtained as a result of interaction with the carbon nanoparticle. Major fluctuations were observed in the RMSF of the protein which was between 1.0 and 8.0 Å throughout the entire protein structure as given in Fig. 9b. The interaction details are represented by two panels in Fig. 9c, where the top panel shows the interactions at a given point of time and the bottom panel represents the 4 residues such as Val73, Val75, Pro81, and Pro163 and their interaction along the course of the simulation period. Interaction fractions of each of these residues are given in the histogram in Fig. 9d, where Pro81 has the highest interaction fraction and Val73 has the least. Ligand RMSF is about 4.0 Å throughout the carbon atoms (Fig. 9e), as a result of its interactions involved in the complex. Residues such as Ile75, Pro81, and Pro163 interact with the protein for more than 10% of the simulation period, represented in Fig. 9f. The structural changes of protein and ligand throughout the simulation period are given in Supplementary figs. S9 & S10. Therefore, this confirms that the interactions are dynamically stable in the applied simulation conditions.

Similarly, when the docked interaction complex of the spike protein (PDB ID: 6VSB) and carbon nanotube was simulated, the trajectories were obtained as shown in Fig. 10. The RMSD changes in the protein structure increase constantly from 3.2 to 5.7 Å over 100 ns as a result of being involved in the binding event, as depicted in Fig. 10a. The plot of protein RMSF which is given in Fig. 10b, shows very high fluctuations

throughout the protein structure ranging from 2.0 to 8.0 Å, indicating the effect of a nanotube on the receptor structure. The interaction plots are given in Fig. 10c, where the top panel represents the contacts and the bottom panel represents the 19 interacting amino acids at a given point of time. The prominent interactions involved the residues Lys310, Tyr313, Pro665, Val772, and Lys776. The interaction fraction for each of the residues was plotted using a histogram as shown in Fig. 10d. It can be observed that the aforementioned amino acids showed ~1.0 (and above) fraction of interaction supporting the previous statement. The ligand RMSF fluctuates between 3.0 and 4.5 Å (Fig. 10e), as the atoms break down during the interaction to inhibit the protein structure. The interaction plot showing the most prominent interaction that occurs greater than 10% of the simulation time is shown in Fig. 10f. The changes that occur to the structures of protein and ligand are shown in Supplementary figs. S11 & S12. Overall, the docked complex interactions and energies are observed to be dynamically stable.

The trajectories obtained for RdRp (PDB ID: 6M71) in complex with nanotube confirmed that the interactions exhibited on docking were stable. The protein RMSD, as shown in Fig. 11a, deviated between 2.0 and 4.0 Å throughout the simulation. The RMSD was below 4.0 Å till about 70 ns, there on it increased and then decreased gradually, as a result of the binding event that occurs between the nanoparticle and the macromolecule. Protein RMSF showed extremely high fluctuations ranging from 0.7 to >5.6 Å along the entire length of the receptor

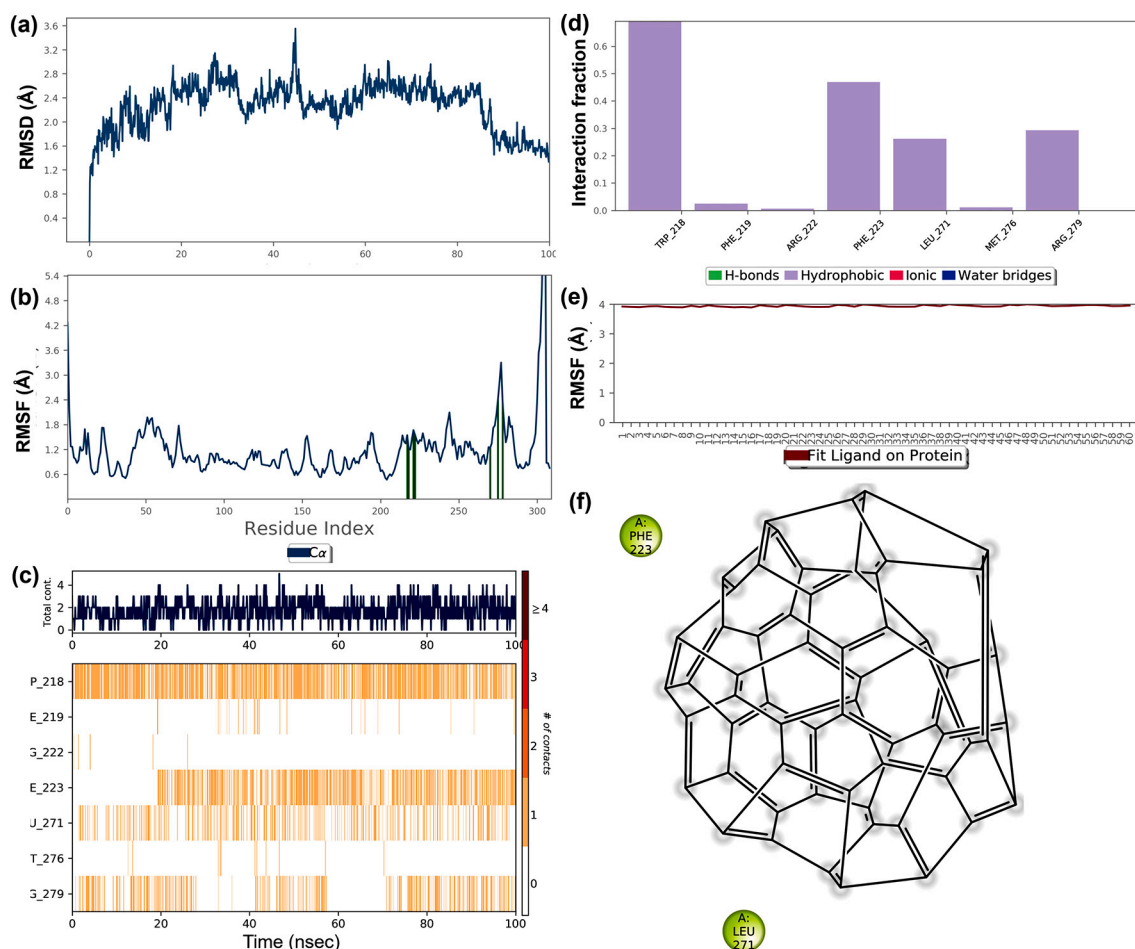


Fig. 7. The MD simulation trajectories of the main protease and nano fullerene complex (a) RMSD: Protein RMSD (Å) on the y-axis and time on the x-axis (b) Protein RMSF (Å) on the y-axis and residues on the x-axis (c) Protein-ligand contacts over the simulation course, (d) histogram representing interaction fraction on the y-axis and residues on the x-axis (e) Ligand RMSF (Å) on the y-axis and atoms on the x-axis and (f) Major interactions that occur during MD simulation.

backbone, which represents the effect of the drug interaction with the target and is depicted in Fig. 11b. The interactions that occurred during the simulation are shown in Fig. 11c, to time. The top panel represents total contacts that occurred throughout the simulation which is depicted to be an average of 5 to 8 interactions at any given point in time. From the bottom panel, it can be observed that 16 residues constantly interacted with the ligand, out of which 4 residues such as Phe35, Val42, Phe48, and Lys50 were involved in prominent interactions. A histogram representing the interacting residues on the x-axis and interaction fraction on the y-axis is shown in Fig. 11d. From this complex, only hydrophobic interactions were observed, and the 4 mentioned residues have an interaction fraction of >0.8 towards the ligand which confirms the stability of the complex interaction. Ligand RMSD fluctuation is shown in Fig. 11e, and it is observed to be >6.0 Å as the ligand atoms undergo significant changes during the interaction events. The interactions that occurred for greater than 10% of the simulation period are shown in Fig. 11f, which included the interaction with the residue Val42. The structural changes undergone by the target and ligand are shown in Supplementary figs. S13 & S14. Overall, the docked complex and the interactions involved were observed to be stable in the applied dynamic conditions.

The main protease (PDB ID: 6LU7) and nanotube complex trajectories obtained from the MD simulation are given in Fig. 12. The RMSD of the receptor protein was observed to be increasing linearly from 1.3 to 3.2 Å along the course of the simulation, as shown in Fig. 12a. The RMSF of the receptor was also obtained with fluctuations as high as 5.5 Å in N-terminal region, whereas the remaining structure fluctuated between

0.6 and 2.9 Å as shown in Fig. 12b. These fluctuations imply that the ligand has a significant effect on suppressing the receptor thereby inhibiting its function. The interactions and the amino acids involved in the interaction are shown in two different panels concerning time in Fig. 12c. The top panel indicates the total number of interactions throughout the simulation course which on average is about 8 for the first half and 10 for the second half of the simulation, whereas the bottom panel represents the 22 residues interacting with nanotube to time, out of which 5 residues such as Tyr154, Val212, Pro252, Phe294 and Val297 interact constantly compared to the other amino acids. The interaction fraction of each of the interacting residues is depicted using a histogram in Fig. 12d. All the observed contacts are hydrophobic and the 5 aforementioned residues have >0.5 interaction involvement. The ligand RMSF is >5.0 Å with extreme fluctuations as a result of the atoms being broken down during the binding event as shown in Fig. 12e. The binding contact that occurs for more than 10% of the simulation period is pictorially represented in Fig. 12f, and Val212 was the residue involved. The structural and chemical changes that the target and ligand undergo throughout 100 ns are shown in Supplementary figs. S15 & S16. Altogether, it is evident that the docked complex and the dynamic interactions involved are relatively stable.

The simulation results obtained for the papain-like protease (PDB ID: 6W9C) and nanotube complex are shown in Fig. 13. The RMSD changes in the protein structure increase constantly from 1.4 to 5.6 Å over 100 ns with an unusual peak between 15 and 20 ns, as a result of being involved in the binding event, as depicted in Fig. 13a. The plot of protein RMSF which is given in Fig. 13b, shows very high fluctuations throughout the

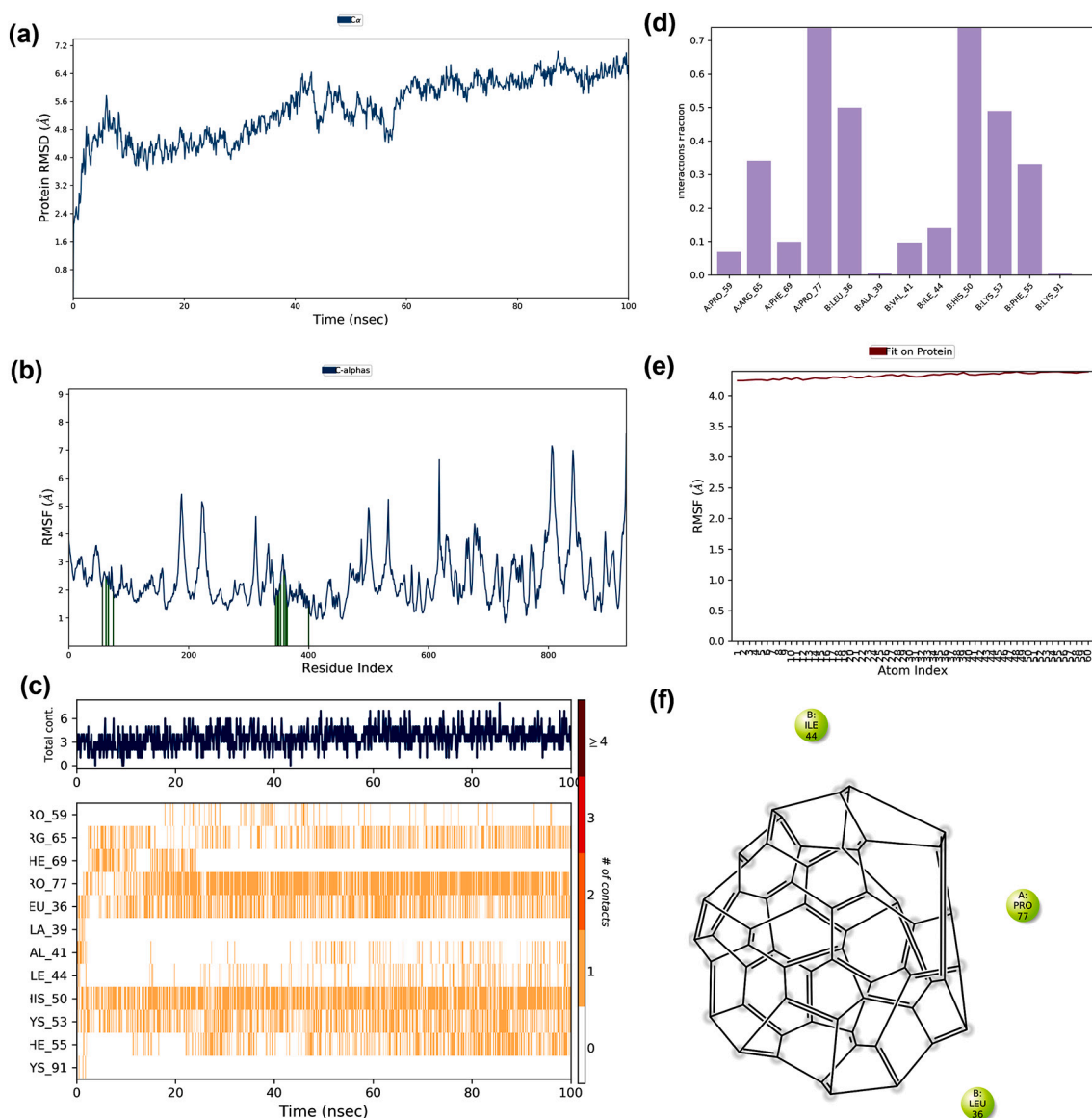


Fig. 8. The MD simulation trajectories of papain – like protease and nano fullerene complex (a) RMSD: Protein RMSD (Å) on the y-axis and time on the x-axis (b) Protein RMSF (Å) on the y-axis and residues on the x-axis (c) Protein-ligand contacts over the simulation course, (d) histogram representing interaction fraction on the y-axis and residues on the x-axis (e) Ligand RMSF (Å) on the y-axis and atoms on the x-axis and (f) Major interactions that occur during MD simulation.

protein structure ranging from 0.8 to 7.2 Å, indicating the effect of a nanotube on the receptor structure. It can be observed that the fluctuations are high at the terminal regions and the beta-sheet regions of the macromolecule. The interaction plots are given in Fig. 13c, where the top panel represents the contacts and the bottom panel represents the 17 interacting amino acids. The prominent interactions involved the residues Phe69, Arg82, Lys91, and Lys175. The interaction fraction for each of the residues was plotted using a histogram as shown in Fig. 13d. It can be observed that the aforementioned amino acids showed ~0.6 (and above) fraction of interaction supporting the previous statement. The ligand RMSF highly fluctuates between 2.5 and > 3.5 Å (Fig. 13e), as the atoms break down during the interaction to inhibit the protein structure. The interaction plot showing the most prominent interaction that occurs greater than 10% of the simulation time is shown in Fig. 13f. The changes that occur to the structures of protein and ligand are shown in Supplementary figs. S17 & S18. Overall, the docked complex interactions and energies are observed to be stable.

The RNA binding domain of the nucleocapsid protein structure is complex with nanotube when simulated generated trajectories as shown

in Fig. 14. The protein RMSD initially increased to about 6.0 Å and decreased to 3.0 Å in the first 13 ns, and then increased to 9.0 Å in the next 10 ns, and there on, remained stable between 7.5 and 9.0 Å as shown in Fig. 14a. This high RMSD is obtained as a result of interaction with the carbon nanoparticle. Major fluctuations were observed in the RMSF of the protein which was between 1.0 and 10.5 Å throughout the entire protein structure as given in Fig. 14b. High fluctuations are observed at the terminal regions. The interaction details are represented by two panels in Fig. 14c, where the top panel shows the interactions at a given point of time and the bottom panel represents the 12 residues and their interaction along the course of the simulation period out of which Leu168, Lys170, Tyr173, and Ala174 were the significant ones. Interaction fractions of each of these residues are given in the histogram in Fig. 14d, where Lys170 showed the highest fraction of 1.4. Ligand RMSF is extremely fluctuating between 4.0 and 7.0 Å throughout the carbon atoms (Fig. 14e), as a result of its interactions involved in the complex. The residue Ala174 interacts with the protein for more than 10% of the simulation period, represented in Fig. 14f. The structural changes of protein and ligand throughout the simulation period are given in

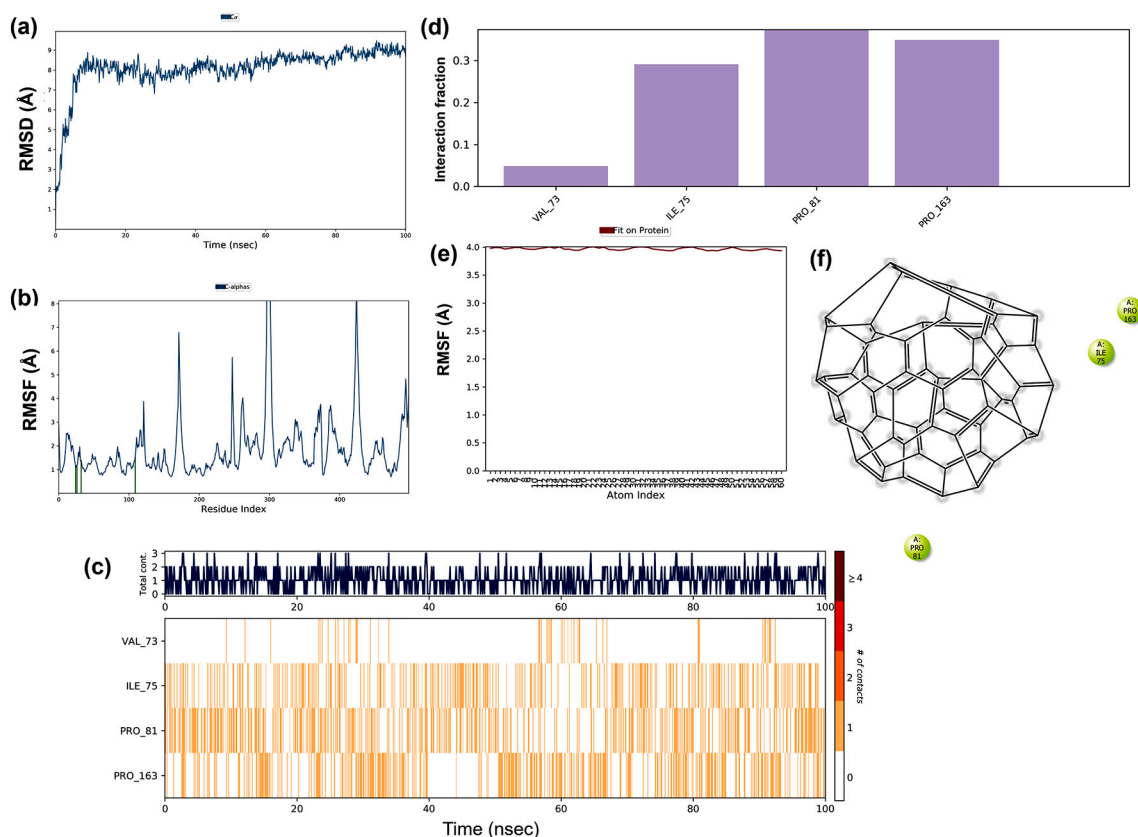


Fig. 9. The MD simulation trajectories of RNA binding domain of the nucleocapsid protein and nano fullerene complex (a) RMSD: Protein RMSD (Å) on the y-axis and time on the x-axis (b) Protein RMSF (Å) on the y-axis and residues on the x-axis (c) Protein-ligand contacts over the simulation course, (d) histogram representing interaction fraction on the y-axis and residues on the x-axis (e) Ligand RMSF (Å) on the y-axis and atoms on the x-axis and (f) Major interactions that occur during MD simulation.

Supplementary figs. S19 & S20. Therefore, this confirms that the interactions are dynamically stable in the applied simulation conditions.

Although both the nanoparticles show promising binding towards SARS-CoV-2 targets and are dynamically stable, it can be observed that carbon nanotube exhibits significantly higher and better binding energy compared to that of carbon nano fullerene. The stability of the structures and interactions increase with higher binding affinity. In our previous studies, we analyzed the interaction energy between conventional drugs such as chloroquine, hydroxychloroquine, favipiravir, ritonavir, lopinavir, and remdesivir and their targets, we observed good interaction energies (Skariyachan et al., 2020; Skariyachan et al., 2021). However, it was significantly lower than the interaction energies observed in the case of carbon nanoparticles which would be taken advantage of to be employed in the treatment of infections associated with SARS-CoV-2.

In the process of identification of protease inhibitors that could be employed against the SARS-CoV-2's Mpro molecular target, Motiwale et al. proposed 6 molecules with the binding affinity >8.5 kcal/mol Mpro, such as N-(4-(((4Z)-5-oxo-1,3-diphenyl-4,5-dihydro-1H-pyrazol-4-ylidene)methyl)phenyl)acetamide, 5-amino-1-[2-(1-benzothiophene-2-yl)-2-oxoethyl]-2,3-dihydro-1H-indole-2,3-dione, 4-(((4Z)-1-(3-chlorophenyl)-5-oxo-3-phenyl-4,5-dihydro-1H-pyrazol-4-ylidene)methyl)benzoic acid, 4-(((4Z)-5-oxo-1,3-diphenyl-4,5-dihydro-1H-pyrazol-4-ylidene)methyl)benzoic acid, (4Z)-4-[[4-(dimethylamino)phenyl]methylidene]-1,3-diphenyl-4,5-dihydro-1H-pyrazole-5-one, and 4-(((4Z)-1-(4-chlorophenyl)-5-oxo-3-phenyl-4,5-dihydro-1H-pyrazol-4-ylidene)methyl)benzoic acid. These molecules showed higher binding affinity compared to conventional drugs such as chloroquine and hydroxychloroquine (Motiwale et al., 2020) However, carbon fullerene and nanotubes show much higher binding energy than these molecules making them a better choice for treatment against COVID-19. In a study conducted by Novir and Aram

(2020), they concluded that doped carbon nano fullerene can be a good drug delivery vehicle for chloroquine drugs due to relatively better binding affinity and electronic properties with chloroquine for the treatment of COVID-19 (Novir and Aram, 2020).

Compared to the aforementioned study, it can also be observed that the binding affinity of carbon fullerene and nanotube with protein targets in our study is significantly higher. In comparison to the studies previously reported, molecules such as Cangrelor, NADH, FAD, Iomeprol, and Tiludronate docked against Spike glycoprotein showed (less than -11.5 kcal/mol) lesser binding energy compared to that of the nanoparticles prioritized in the current study. Similarly, molecules such as Zanamivir, Bortezomib, Saquinavir, Indinavir, Cangrelor, Remdesivir, and FAD docked against the main protease exhibited (less than -11.01 kcal/mol) lesser binding energy compared to the nanoparticles (Hall Jr and Ji, 2020). The suggested drugs against COVID19 such as chloroquine, remdesivir, ribavirin, luteolin, and N3 inhibitor showed binding energy less than -11.0 kcal/mol against spike protein, RdRp, main protease, and papain-like protease (Yu et al., 2020). Natural component derivatives from plants such as *Withania somnifera*, *Somniferine*, *Tinospora cordifolia* (Giloy), and *Ocimum sanctum* (Tulsi) were docked against the main protease exhibited lesser binding energy compared to that of the nanoparticles (Shree et al., 2020; Satyendra, 2020). Therefore, it is evident that the carbon nanoparticles employed in this study exhibited better binding energy towards the prioritized SARS-CoV-2 targets. There are several studies recently published on the binding potential of carbon-based nanomaterials towards viruses and helps in the detection of viral pathogens or as antiviral agents to viral pandemics including COVID19 (Reina et al., 2020; Shao et al., 2021; Serrano-Aroca et al., 2021; Jomhori et al., 2021; Riley and Narayan, 2021).

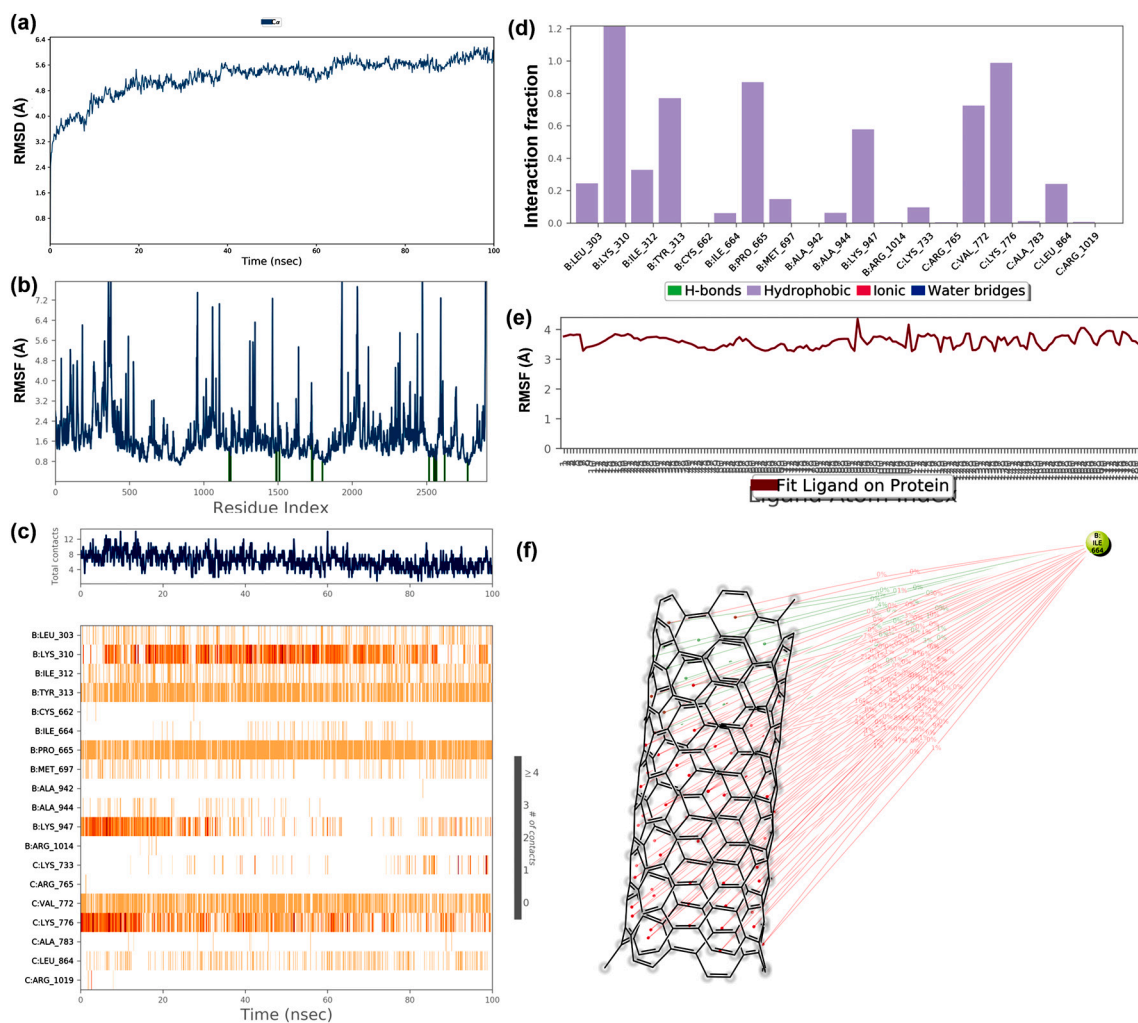


Fig. 10. The MD simulation trajectories of spike protein and nanotube complex (a) RMSD: Protein RMSD (Å) on the y-axis and time on the x-axis (b) Protein RMSF (Å) on the y-axis and residues on the x-axis (c) Protein-ligand contacts over the simulation course, (d) histogram representing interaction fraction on the y-axis and residues on the x-axis (e) Ligand RMSF (Å) on the y-axis and atoms on the x-axis and (f) Major interactions that occur during MD simulation.

In the present study, we have modeled the interaction of one major orientation of five different sites of SARS-CoV-2 targets with SWCNT and nano-fullerene from molecular docking. It is not persuasive that these targets only adopt this orientation in adsorption on hydrophobic surfaces. There are possibilities of multiple orientations in adsorption on charged or hydrophobic surfaces. Thus, it is important to understand the interaction modeling of multiple orientations. As there are no data available on the actual targets of the nanomaterials used, the present study prioritized the selected SARS-CoV-2 as putative molecular targets, and the study made the conclusion based on interaction modeling and MD simulation, thus, the specificity of nanoparticles towards these targets should be validated by experimentally. Further, the MD simulations were performed at 100 ns, for all five complexes. It is suggested to perform the MD simulation for a longer time duration probably 500 ns for getting concurrent interaction profile and stability of the complexes. Thus, the current study provides a profound insight into the molecular interactions and binding events of the nanoparticles and the multiple targets of SARS-CoV-2. The data and conclusions suggested in the present study are based on the web-based database and bioinformatics software and server with the lack of solid molecular biology experiments to confirm these carbon nanomaterials binding targets, SARS-CoV-2 Spike, RdRp, main protease, papain-like protease, and nucleocapsid protein, thus, further experimental studies and validations are essential to conclude. However, the current study provides a fundamental basis

for carrying out *in vitro* assays and further experimental validations.

3. Conclusion

Despite the reported toxicity of the nanoparticles, they could be used as potential leads for inhibiting the SARS-CoV-2 targets, as the ADME properties obtained from the computational predictions are similar to those exhibited by many of the currently prescribed drugs. They are also known to be effective for target-specific treatments, drug delivery systems, cancer-associated treatments, and so on. To address the emergent requirement of an alternative therapeutic solution to control the global pandemic of SARS-CoV-2, the binding potential of carbon nano fullerene and nanotubes against major SARS-CoV-2 targets such as spike proteins, RdRp, main protease, papain-like protease, and RNA binding domain of the nucleocapsid protein were predicted. Molecular docking studies revealed that carbon nano fullerene and carbon nanotubes exhibited better binding energy than the currently suggested antiviral drugs. The MD simulation studies confirmed that the dynamic interactions between prioritized targets and nanomaterials were identified to be stable and potential. Among the two carbon nanoparticles, nanotubes exhibited better binding energy (kcal/mol) when compared to carbon fullerene. Therefore, it could be suggested that these nanoparticles are probably employed as potential lead molecules against multiple targets of SARS-CoV-2 with further experimental studies and validations.

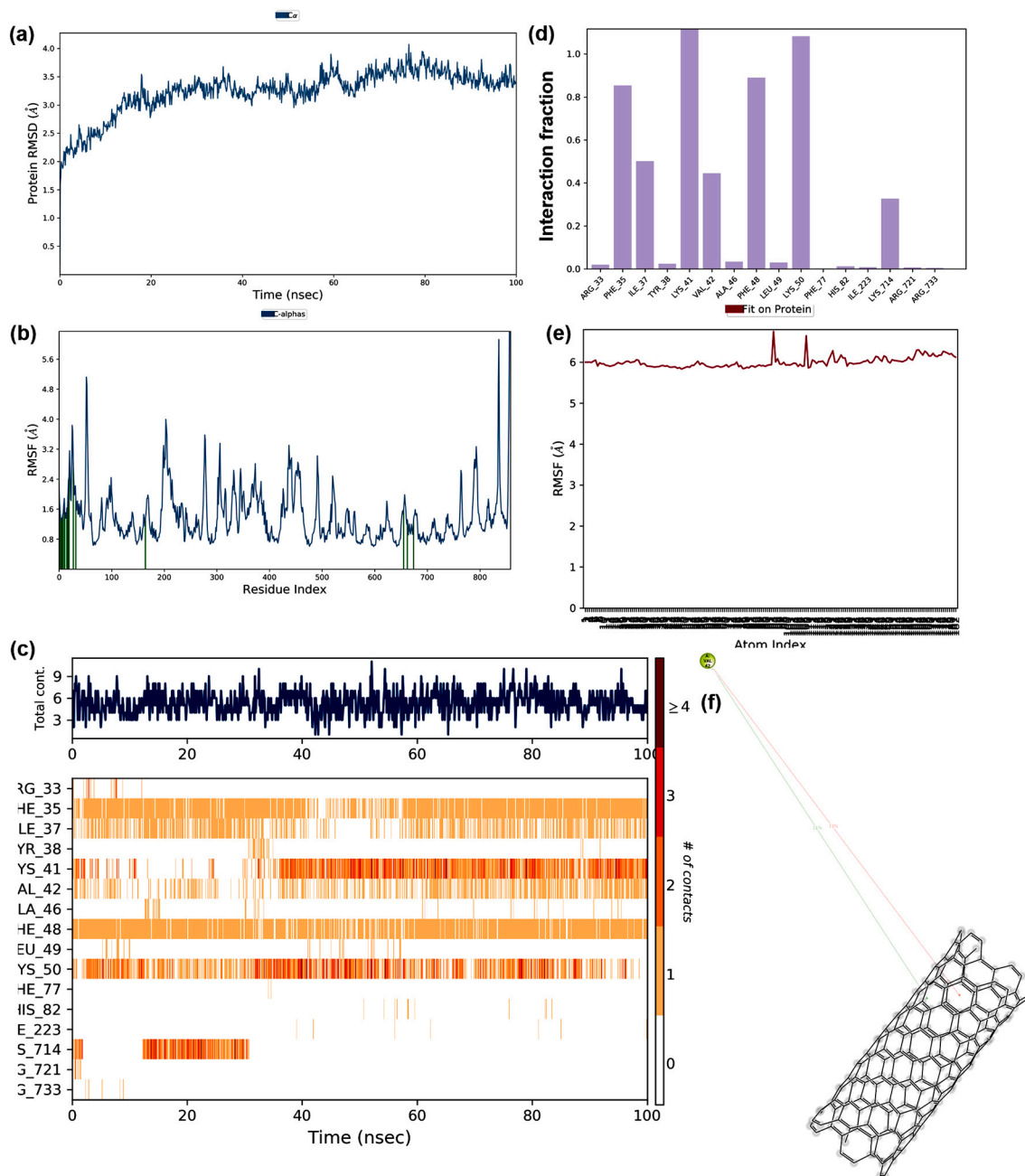


Fig. 11. The MD simulation trajectories of RdRp protein and nanotube complex (a) RMSD: Protein RMSD (Å) on the y-axis and time on the x-axis (b) Protein RMSF (Å) on the y-axis and residues on the x-axis (c) Protein-ligand contacts over the simulation course, (d) histogram representing interaction fraction on the y-axis and residues on the x-axis (e) Ligand RMSF (Å) on the y-axis and atoms on the x-axis and (f) Major interactions that occur during MD simulation.

4. Methods

4.1. Identification of putative targets

Five major virulent proteins were analyzed and selected as targets based on their involvement in the pathogenicity of SARS-CoV-2. Literature from databases such as PubMed and UniProt (The UniProt Consortium, 2019) was utilized for the identification of these probable putative targets. Experimentally solved three-dimensional structures of the identified protein targets were retrieved from the RCSB PDB (Berman et al., 2020). The targets that were retrieved included Cryo-electron microscopy structure of Spike glycoprotein (PDB ID: 6VSB) (Wrapp et al., 2020), electron microscopy structure of RNA dependent RNA polymerase (PDB ID: 6M71) (Gao et al., 2020b), X-ray diffraction

structures of main protease (PDB ID: 6LU7), papain-like protease (PDB ID: 6W9C) (Jin et al., 2020) and RNA binding domain of the Nucleocapsid protein (PDB ID: 6M3M) (Kang et al., 2020).

4.2. Modeling and retrieval of nano-structures

The 3-D chemical structure of carbon nano-fullerene, C60 (PubChem ID: 123591) was retrieved from the PubChem database (Kim et al., 2019). The 3-D chemical structure of carbon nanotube was modeled using Nanotube Modeller (www.jcrystal.com/products/wincnt/). This carbon nanotube was modeled based on the literature evidence of the dimensions used for medicinal purposes. Therefore, carbon nanotube (C182) with (6, 5) chirality of length 20.0 Å, the diameter of 7.474 Å, the bond length of 1.421 Å, and 261 bonds were selected.

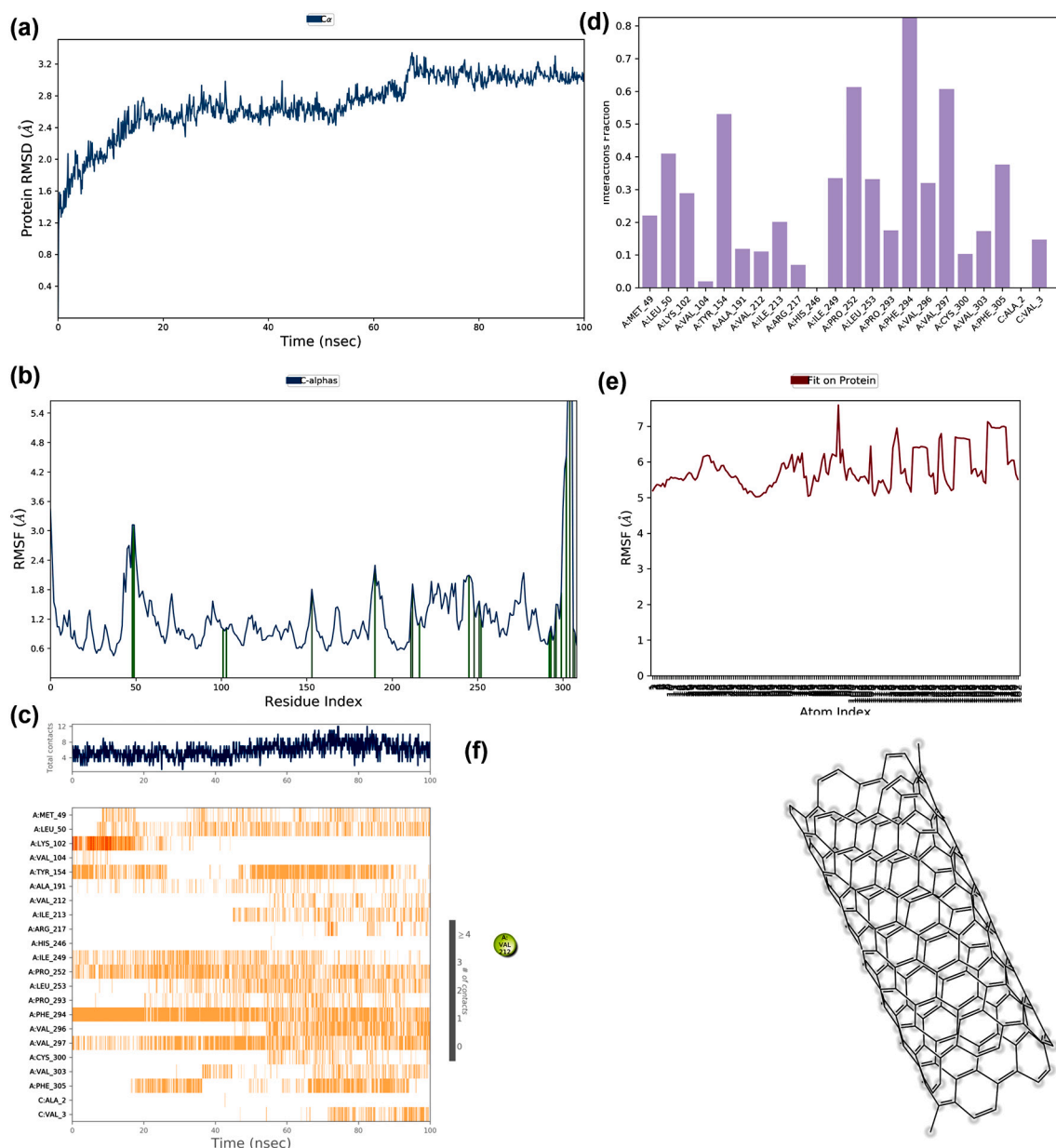


Fig. 12. The MD simulation trajectories of main protease and nano tube complex (a) RMSD: Protein RMSD (Å) on the y-axis and time on the x-axis (b) Protein RMSF (Å) on the y-axis and residues on the x-axis (c) Protein-ligand contacts over the simulation course, (d) histogram representing interaction fraction on the y-axis and residues on the x-axis (e) Ligand RMSF (Å) on the y-axis and atoms on the x-axis and (f) Major interactions that occur during MD simulation.

4.3. Drug likeness and pharmacokinetic features of carbon nanoparticles

The computational biology tools such as PreADMET (Veber et al., 2002) and admetSAR (Cheng et al., 2019) were utilized for the prediction of drug-likeness, pharmacological, and toxicity features of the carbon nano fullerene and nanotubes used in this study. Descriptors such as Lipinski rule of five (Lipinski et al., 2001), Comprehensive Medicinal Chemistry (CMC) rule, MDL Drug Data Report (MDDR) like rule (Frimurer et al., 2000), World drug indexes (WDI) like rule, and lead-like rule (Ajay et al., 1998) were employed for the prediction of drug-likeness. Molecular models used for the prediction of absorption, distribution, metabolism, and excretion (ADME) included plasma protein binding, blood-brain barrier (BBB) (Ajay et al., 1999), skin permeability, human intestinal absorption (HIA), Madin-Darby canine kidney (MDCK) cell permeability (Irvine et al., 1999), oral bioavailability and caco2 cell permeability (Yazdanian et al., 1998), toxicity prediction included models for fish toxicity, daphnia toxicity, hERG inhibition, rodent

carcinogenicity, Ames test (Mortelmans and Zeiger, 2000), mutagenicity in different strains of *Salmonella typhimurium* models.

4.4. Molecular docking

Autodock vina (Dai et al., 2020) was employed to perform docking of the carbon nanoparticles against the identified target proteins. The binding sites of the protein targets were predicted using Depth (Tan et al., 2011) and CastP (Binkowski et al., 2003) servers. The 3-D structures of the protein targets and the carbon nanoparticles were prepared using the Autodock tool of the MGL tools package (Morris et al., 2009) according to the Autodock vina protocol (Schrödinger Release 2019–3: Desmond Molecular Dynamics System, 2019). The torsion, number of torsions, and root atoms for the ligands were assigned and the file was saved as pdbqt. Similarly, the targets were prepared by removing all the heteroatoms and ligands from the PDB files and polar hydrogen atoms were added to the targets. The target was saved in pdbqt format. The

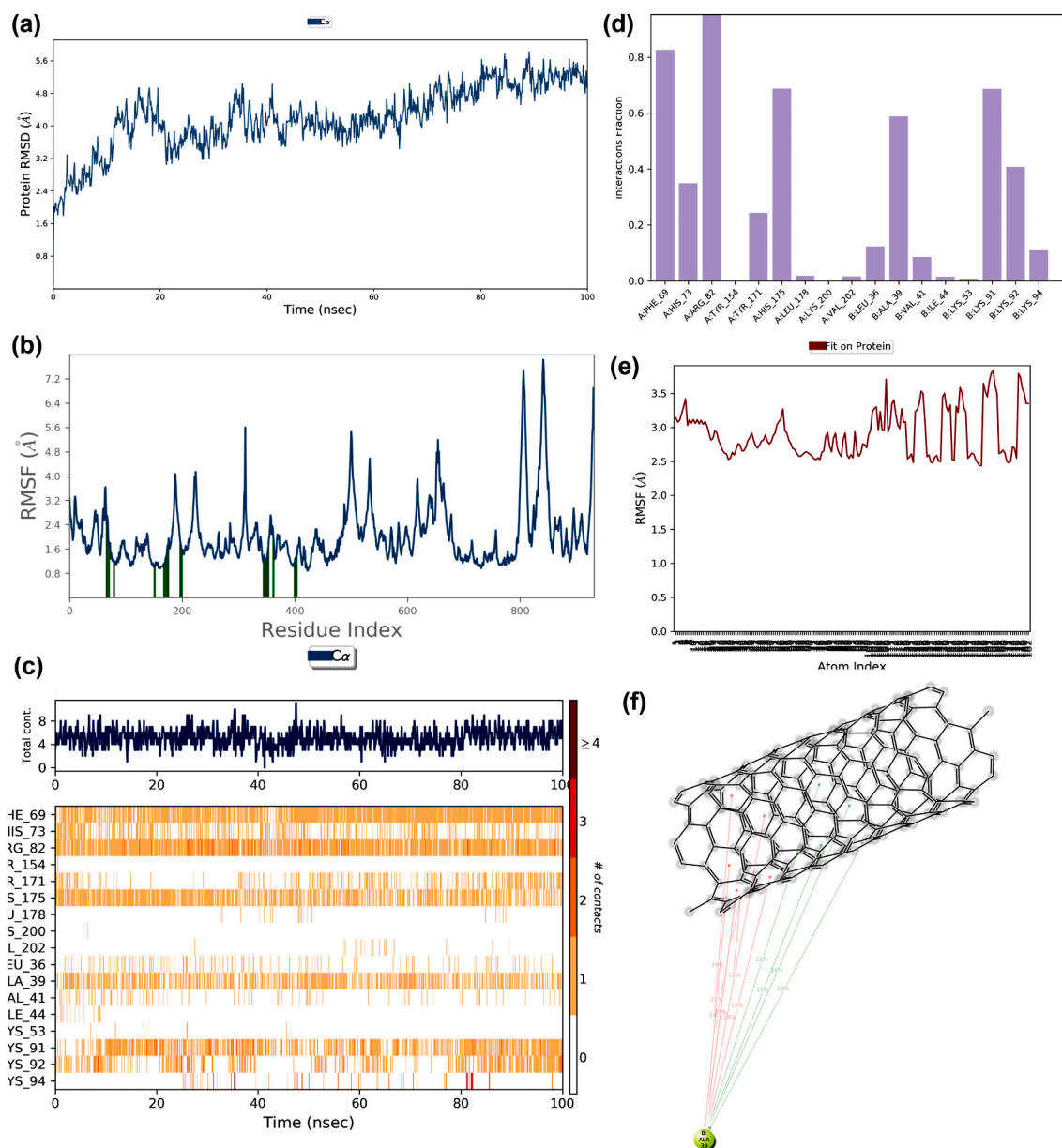


Fig. 13. The MD simulation trajectories of papain – like protease and nano tube complex (a) RMSD: Protein RMSD (Å) on the y-axis and time on the x-axis (b) Protein RMSF (Å) on the y-axis and residues on the x-axis (c) Protein-ligand contacts over the simulation course, (d) histogram representing interaction fraction on the y-axis and residues on the x-axis (e) Ligand RMSF (Å) on the y-axis and atoms on the x-axis and (f) Major interactions that occur during MD simulation.

selected targets of SARS-CoV-2 were kept rigid and the ligands were kept flexible during the docking simulation. The grid box parameters were assigned for the target proteins and the resulting interactions between the targets and the nanoparticles along with their binding energies and RMSD were interpreted and analyzed.

4.5. Molecular dynamic simulation

The best-docked complexes were subjected to molecular dynamic simulation by the Desmond module of Schrödinger's suite [77] to test the stability of the interactions. Hydrogen bonds were assigned to the protein and nanoparticles in the complex. The MD simulation was carried out by Optimized Potentials for Liquid Simulations (OPLS) force field and solid polymer electrolyte (SPE) water models at 300 K using the constant number of particles, pressure, and temperature (NPT) ensemble class for 100 ns. The trajectories of RMSD, RMSF, protein-ligand contacts, ligand properties, and ligand torsion profile were obtained and

analyzed.

The obtained trajectories of RMSD and RMSF were calculated using the following formula:

$$RMSD_x = \sqrt{\frac{1}{N} \sum_{i=1}^N (r_i^x(t_x) - r_i(t_{ref}))^2}$$

$$\& RMSF_i = \sqrt{\frac{1}{T} \sum_{t=1}^T \langle (r_i^x(t) - r_i(t_{ref}))^2 \rangle}$$

Where N is the number of atoms, t_{ref} is the reference time (t = 0), r_i is the position of atom i in the reference at time t_{ref}, r_i is the position of the selected atoms in frame x, where frame x is recorded at time t_x and T is the trajectory time.

Author contribution

SS and DG designed the hypothesis, framed and standardized the methodology, and performed major parts of the work. DG, DD, and AJ performed the molecular docking. AU and VN performed molecular dynamic simulation studies and analyses. SS finally reviewed and edited

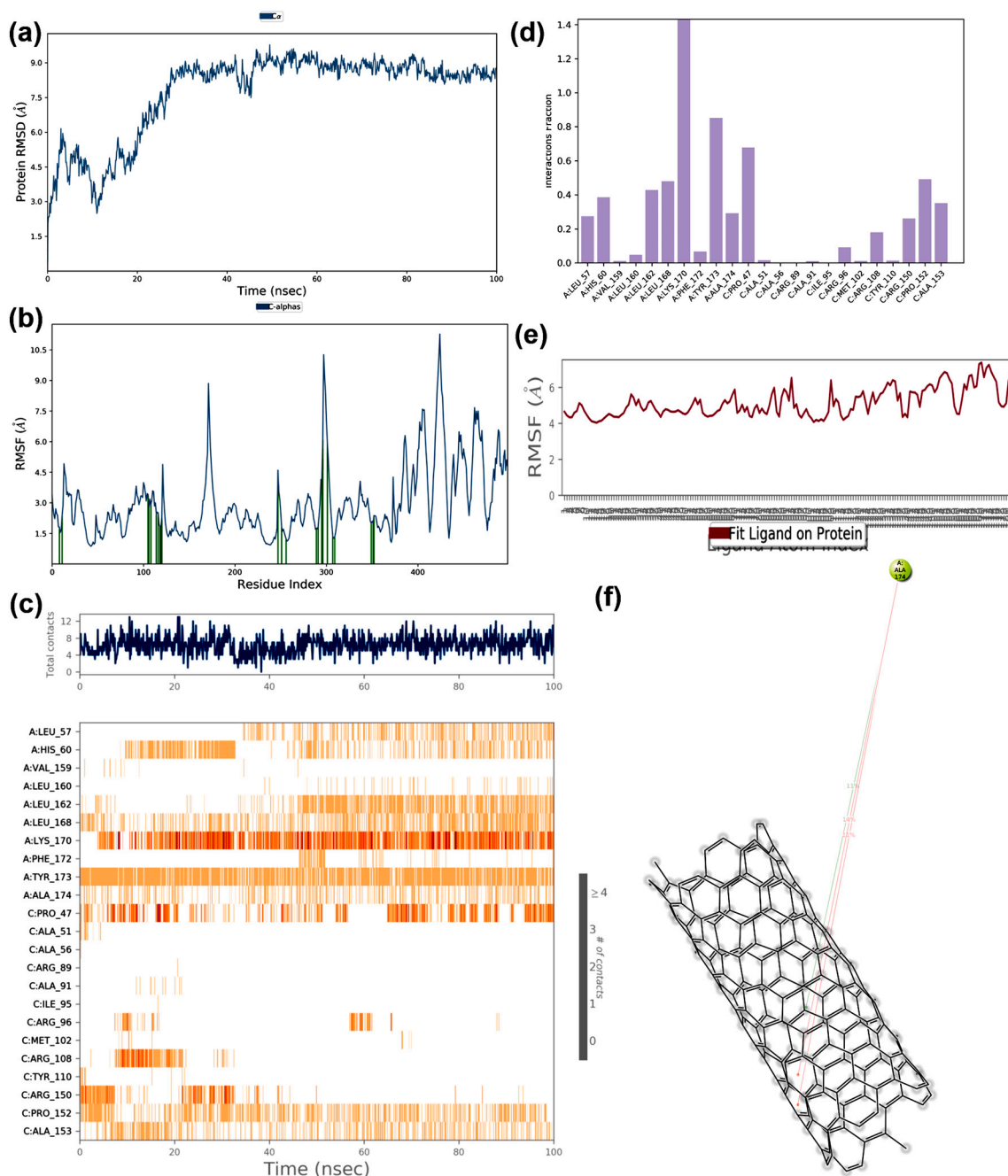


Fig. 14. The MD simulation trajectories of RNA binding domain of the nucleocapsid protein and nano tube complex (a) RMSD: Protein RMSD (Å) on the y-axis and time on the x-axis (b) Protein RMSF (Å) on the y-axis and residues on the x-axis (c) Protein-ligand contacts over the simulation course, (d) histogram representing interaction fraction on the y-axis and residues on the x-axis (e) Ligand RMSF (Å) on the y-axis and atoms on the x-axis and (f) Major interactions that occur during MD simulation.

the manuscript. All authors carefully read and approved the final version.

Funding

This research did not receive any specific grant from funding agencies in the public, commercial, or not-for-profit sectors.

Data and software availability

The 3-D structure of carbon nano-fullerene, C60 with available at PubChem with PubChem ID: 123591 <https://pubchem.ncbi.nlm.nih.gov/#query=123591>

<https://pubchem.ncbi.nlm.nih.gov/#query=123591>

3-D chemical structure of carbon nanotube modeled by Nanotube Modeller which is available at www.jcrystal.com/products/wincnt/.

The 3D structures of the molecular targets of SARS-CoV used in the present study is available at <https://www.rcsb.org/> with the PDBID: 6VSB, 6M71, 6LU7, 6W9C, 6M3M

The virtual screening of the ligand is carried out by PreADMET, which is available at <https://preadmet.bmdrc.kr/>

The 3D structure The AutoDock Vina (version 1.1.2) used for molecular docking can be downloaded free of charge <http://vina.scripps.edu/download.html>. The associated MGL tool can be downloaded from <http://mgltools.scripps.edu/downloads>.

The Desmond Molecular Dynamics System of the Schrödinger Release 2019–3 was used for MD simulations (<https://www.schrodinger.com/products/desmond>).

The UCSF ChimeraX used for 3D model building and visualization is available at <https://www.cgl.ucsf.edu/chimerax/>

Declaration of Competing Interest

The authors declare no conflict of interest

Appendix A. Supplementary data

Supplementary data to this article can be found online at <https://doi.org/10.1016/j.meegid.2021.105155>.

References

- Aftab, S.O., Ghouri, M.Z., Masood, M.U., Haider, Z., Khan, Z., Ahmad, A., Munawar, N., 2020. Analysis of SARS-CoV-2 RNA-dependent RNA polymerase as a potential therapeutic drug target using a computational approach. *J. Transl. Med.* 18, 1–15.
- Ajay, A., Walters, P., Murcko, A., 1998. Can we learn to distinguish between “drug-like” and “non-drug-like” molecules? *J. Med. Chem.* 41, 3314–3321.
- Ajay, A., Bemis, W., Murcko, A., 1999. Blood brain barrier: design in libraries with CNS activity. *J. Med. Chem.* 42, 4942–4951.
- Ali, I., Alharbi, O.M., 2020. COVID-19: disease, management, treatment, and social impact. *Sci. Total Environ.* 138861.
- Altuleta, D., Maassen, S., Baranov, M.V., van den Bogaart, G., 2021. What makes (hydroxy)chloroquine ineffective against COVID-19: insights from cell biology. *J. Mol. Cell Biol.* 175, 184. <https://doi.org/10.1093/jmcb/mjab016>.
- Berman, H.M., Westbrook, J., Feng, Z., Gilliland, G., Bhat, T.N., Weissig, H., Shindyalov, I.N., Bourne, P.E., 2020. The Protein Data Bank. *Nucleic Acids Res.* 28, 235–242.
- Bhavana, V., Thakor, P., Singh, S.B., Mehra, N.K., 2020. COVID-19: pathophysiology, treatment options, nanotechnology approaches, and research agenda to combating the SARS-CoV2 pandemic. *Life Sci.* 118336.
- Binkowski, T.A., Naghibzadeh, S., Liang, J., 2003. CASTp: computed atlas of surface topography of proteins. *Nucleic Acids Res.* 31, 3352–3355.
- Casella, M., Rajnik, M., Cuomo, A., Dulebohn, S.C., Di Napoli, R., 2021. Features, evaluation and treatment coronavirus (COVID-19). In: *StatPearls*. StatPearls Publishing.
- Cheng, F., Li, W., Zhou, Y., Shen, J., Wu, Z., Liu, G., Lee, P.W., Tang, Y., 2019. Correction to “admetSAR: a comprehensive source and free tool for assessment of chemical ADMET properties”. *J. Chem. Info. Model.* 59, 4959.
- Cong, Y., Ulasli, M., Schepers, H., Mauthe, M., V’kovski, P., Kriegenburg, F., Thiel, V., de Haan, C.A.M., Reggiori, F., 2020. Nucleocapsid protein recruitment to replication-transcription complexes plays a crucial role in coronavirus life cycle. *J. Virol.* 94.
- Dai, L., Gao, G.F., 2021. Viral targets for vaccines against COVID-19. *Nat. Rev. Immunol.* 21, 73–82.
- Dai, W., Zhang, B., Jiang, X.M., Su, H., Li, J., Zhao, Y., Xie, X., Jin, Z., Peng, J., Liu, F., Li, C., Li, Y., Bai, F., Wang, H., Cheng, X., Cen, X., Hu, S., Yang, X., Wang, J., Liu, X., Xiao, G., Jiang, H., Rao, Z., Zhang, L.K., Xu, Y., Yang, H., Liu, H., 2020. Structure-based design of antiviral drug candidates targeting the SARS-CoV-2 main protease. *Science* 368, 1331–1335.
- Dutta, N.K., Mazumdar, K., Gordy, J.T., 2020. The Nucleocapsid protein of SARS-CoV-2: a target for vaccine development. *J. Virol.* 94 (e00647-20).
- Frimurer, T., Bywater, R., Nærum, L., Lauritsen, L., Brunak, S., 2000. Improving the odds in discriminating “drug-like” from “non-drug-like” compounds. *J. Chem. Info. Comput. Sci.* 40, 1315–1324.
- Gao, X., Qin, B., Chen, P., Zhu, K., Hou, P., Wojdyla, J.A., Wang, M., Cui, S., 2020a. Crystal structure of SARS-CoV-2 papain-like protease. *Acta Pharm. Sin. B* 11, 237–245.
- Gao, Y., Yan, L., Huang, Y., Liu, F., Zhao, Y., Cao, L., Wang, T., Sun, Q., Ming, Z., Zhang, L., Ge, J., Zheng, L., Zhang, Y., Wang, H., Zhu, Y., Zhu, C., Hu, T., Hua, T., Zhang, B., Yang, X., Li, H., Yang, H.Z., Liu, Z., Xu, W., Guddat, L.W., Wang, Q., Lou, Z., Rao, Z., 2020b. Structure of the RNA-dependent RNA polymerase from COVID-19 virus. *Science* 368, 779–782.
- Gao, Z., Xu, Y., Sun, C., Wang, X., Guo, Y., Qiu, S., Ma, K., 2021. A systematic review of asymptomatic infections with COVID-19. *J. Microbiol. Immunol. Infect.* 54, 12–16.
- Hall Jr., D.C., Ji, H.F., 2020. A search for medications to treat COVID-19 via in silico molecular docking models of the SARS-CoV-2 spike glycoprotein and 3CL protease. *Travel Med. Infect. Dis.* 35, 101646.
- Han, H.J., Nwagwu, C., Anyim, O., Ekwereamadu, C., Kim, S., 2021. COVID-19 and cancer: from basic mechanisms to vaccine development using nanotechnology. *Int. Immunopharmacol.* 90, 107247.
- Irvine, D., Takahashi, L., Lockhart, K., Cheong, J., Tolan, W., Selick, E., Grove, R., 1999. MDCK (Madin-Darby canine kidney) cells: a tool for membrane permeability screening. *J. Pharma. Sci.* 88, 28–33.
- Jin, Z., Du, X., Xu, Y., Deng, Y., Liu, M., Zhao, Y., Zhang, B., Li, X., Zhang, L., Peng, C., Duan, Y., Yu, J., Wang, L., Yang, K., Liu, F., Jiang, R., Yang, X., You, T., Liu, X., Yang, X., You, Y.T., Liu, X., Yang, X., Bai, F., Liu, H., Liu, X., Guddat, L.W., Xu, W., Xiao, G., Qin, C., Shi, Z., Jiang, H., Yang, Z.R.H., 2020. Structure of Mpro from SARS-CoV-2 and discovery of its inhibitors. *Nature* 582, 289–293.
- Jomhori, M., Mosaddeghi, H., Farzin, H., 2021. Tracking the interaction between single-wall carbon nanotube and SARS-CoV-2 spike glycoprotein: a molecular dynamics simulations study. *Comput. Biol. Med.* 136, 104692. <https://doi.org/10.1016/j.combiomed.2021.104692>.
- Kang, S., Yang, M., Hong, Z., Zhang, L., Huang, Z., Chen, X., He, S., Zhou, Z., Zhou, Z., Chen, Q., Yan, Y., Zhang, C., Shan, H., Chen, S., 2020. Crystal structure of SARS-CoV-2 nucleocapsid protein RNA binding domain reveals potential unique drug targeting sites. *Acta Pharm. Sin. B* 10, 1228–1238.
- Kannan, S., Ali, P., Shaik Syed, Sheeza, A., Hemalatha, K., 2020. COVID-19 (Novel Coronavirus 2019) - recent trends. *Eur. Rev. Med. Pharmacol. Sci.* (24), 2006–2011.
- Khodadadian, A., Hosseini, K., Manzour-Ol-Ajdad, A., Hedayati, M., Kalantarinejad, R., Heitzinger, C., 2017. Optimal design of nanowire field-effect troponin sensors. *Comput. Biol. Med.* 87, 46–56. <https://doi.org/10.1016/j.combiomed.2017.05.008>.
- Kim, S., Chen, J., Cheng, T., Gindulyte, A., He, J., He, S., Li, Q., Shoemaker, B.A., Thiessen, P.A., Yu, B., Zaslavsky, L., Zhang, J., Bolton, E.E., 2019. PubChem in 2021: new data content and improved web interfaces. *Nucleic Acids Res.* 47, D1388–D1395.
- Krause, P.R., Fleming, T.R., Longini, I.M., Peto, R., Briand, S., Heymann, D.L., et al., 2021. SARS-CoV-2 variants and vaccines. *N. Engl. J. Med.* 385, 179–186. <https://doi.org/10.1056/NEJMsr2105280>.
- Lipinski, C., Lombardo, F., Dominy, B., Feeney, P., 2001. Experimental and computational approaches to estimate solubility and permeability in drug discovery and development settings. *Adv. Drug Deliv. Rev.* 46, 3–26.
- Melanthota, S.K., Banik, S., Chakraborty, I., Pallen, S., Gopal, D., Chakrabarti, S., Mazumder, N., 2020. Elucidating the microscopic and computational techniques to study the structure and pathology of SARS-CoVs. *Microsc. Res. Tech.* 83, 1623–1638.
- Mirsian, S., Khodadadian, A., Hedayati, M., Manzour-Ol-Ajdad, A., Kalantarinejad, R., Heitzinger, C., 2019. A new method for selective functionalization of silicon nanowire sensors and Bayesian inversion for its parameters. *Biosens. Bioelectron.* 142, 111527. <https://doi.org/10.1016/j.bios.2019.111527>.
- Morris, G.M., Huey, R., Lindstrom, W., Sanner, M.F., Belew, R.K., Goodsell, D.S., Olson, A.J., 2009. AutoDock4 and AutoDockTools4: automated docking with selective receptor flexibility. *J. Comput. Chem.* 30, 2785–2791.
- Mortelmans, K., Zeiger, E., 2000. The Ames Salmonella/microsome mutagenicity assay. *Mut. Res.* 455, 29–60.
- Mothay, D., Ramesh, K.V., 2020. Binding site analysis of potential protease inhibitors of COVID-19 using AutoDock. *Virus Dis.* 31, 194–199.
- Motiwale, M., Yadav, N.S., Kumar, S., Kushwaha, T., Choudhri, G., Sharma, S., Singour, P.K., 2020. Finding potent inhibitors for COVID-19 main protease (Mpro): an *in silico* approach using SARS-CoV-3CL protease inhibitors for combating CORONA. *J. Biomol. Struct. Dyn.* 1, 12.
- Naserghandi, A., Allameh, S.F., Saffarpour, R., 2020. All about COVID-19 in brief. *New Microbes, New Infect.* 35, 100678.
- Novir, S.B., Aram, M.R., 2020. Quantum mechanical simulation of chloroquine drug interaction with C60 fullerene for treatment of COVID-19. *Chem. Phys. Lett.* 757, 137869.
- Nutho, B., Mahalapbutr, P., Hengphasatporn, K., Pattarangoon, N.C., Simanon, N., Shigetani, Y., Hannongbua, S., Rungrotmongkol, W., 2020. Why are Lopinavir and ritonavir effective against the newly emerged coronavirus 2019? Atomistic Insights into the Inhibitory Mechanisms. *Biochemistry* 59, 1769–1779.
- Palacios Cruz, M., Santos, E., Velázquez Cervantes, M.A., León Juárez, M., 2020. COVID-19, a worldwide public health emergency. *Rev. Clin. Esp.* 221, 55–61.
- Rahimi, F., Abadi, A., Talebi Bezin, 2020. Challenges of managing the asymptomatic carriers of SARS-CoV-2. *Travel Med. Infect. Dis.* 37, 101677.
- Rai, M., Bonde, S., Yadav, A., Bhowmik, A., Rathod, S., Ingle, P., Gade, A., 2021. Nanotechnology as a shield against COVID-19: current advancement and limitations. *Viruses* 13, 1224. <https://doi.org/10.3390/v13071224>.
- Reina, G., Peng, S., Jacquemin, L., Andrade, A.F., Bianco, A., 2020. Hard nanomaterials in time of viral pandemics. *ACS Nano* 14 (8), 9364–9388.
- Riley, P.R., Narayan, R.J., 2021. Recent advances in carbon nanomaterials for biomedical applications: a review. *Curr Opin Biomed Eng.* 17, 100262. <https://doi.org/10.1016/j.cobme.2021.100262>.
- Romeo, A., Iacovelli, F., Falconi, M., 2020. Targeting the SARS-CoV-2 spike glycoprotein prefusion conformation: virtual screening and molecular dynamics simulations applied to the identification of potential fusion inhibitors. *Virus Res.* 286, 198068.
- Saleemi, M.A., Kong, Y.L., Yong, P.V.C., Wong, E.H., 2020. An overview of recent development in therapeutic drug carrier system using carbon nanotubes. *J. Drug Del. Sci. Tech.* 101855.
- Satyendra, M., 2020. Phytochemical efficiency of *Ocimum sanctum* (Tulsi) in health enhancement and disease prevention: a review. *IJARES* 9.
- Shaw Research, D.E., New York, N.Y., Tools, Maestro-Desmond Interoperability (Eds.), 2019. Schrödinger Release 2019–3: Desmond Molecular Dynamics System. Schrödinger, New York, NY.
- Schrödinger Release 2020–4, 2020. Maestro, Schrödinger, LLC, New York, NY.
- Serrano-Aroca, Á., Takayama, K., Tuñón-Molina, A., Seyran, M., Hassan, S.S., Pal Choudhury, P., et al., 2021. Carbon-based nanomaterials: promising antiviral agents to combat COVID-19 in the microbial-resistant era. *ACS Nano* 15 (5), 8069–8086.
- Shao, W., Shurin, M.R., Wheeler, S.E., He, X., Star, A., 2021. Rapid detection of SARS-CoV-2 antigens using high-purity semiconducting single-walled carbon nanotube-based field-effect transistors. *ACS Appl. Mater. Interfaces* 13 (8), 10321–10327.
- Shin, M.D., Shukla, S., Chung, Y.H., Beiss, V., Chan, S.K., Ortega-Rivera, O.A., David, M.W., Angela, C., Markus, S., Jonathan, K.P., Steinmetz, N.F., 2020. COVID-19 vaccine

- development and a potential nanomaterial path forward. *Nat. Nanotechnol.* 15, 646–655.
- Shirasu, K., Kitayama, S., Liu, F., Yamamoto, G., Hashida, T., 2021. Molecular dynamics simulations and theoretical model for engineering tensile properties of single-and multi-walled carbon nanotubes. *Nanomaterials (Basel)*. 11 (3), 795. <https://doi.org/10.3390/nano11030795>.
- Shree, P., Mishra, P., Selvaraj, C., Singh, S.K., Chaube, R., Garg, N., Tripathi, Y.B., 2020. Targeting COVID-19 (SARS-CoV-2) main protease through active phytochemicals of ayurvedic medicinal plants - *Withania somnifera* (Ashwagandha), *Tinospora cordifolia* (Giloy) and *Ocimum sanctum* (Tulsi) - a molecular docking study. *J. Biomol. Struct. Dyn.* 1, 1–14.
- Singh, P., Singh, D., Sa, P., Mohapatra, P., Khuntia, A., Sahoo, S., 2021. Insights from nanotechnology in COVID-19: prevention, detection, therapy and immunomodulation. *Nanomedicine (Lond)*. 16 (14), 1219–1235. <https://doi.org/10.2217/nmm-2021-0004>.
- Skariyachan, S., Gopal, D., Chakrabarti, S., Kempanna, P., Uttarkar, A., Muddebihalkar, A.G., Niranjana, V., 2020. Structural and molecular basis of the interaction mechanism of selected drugs towards multiple targets of SARS-CoV-2 by molecular docking and dynamic simulation studies- deciphering the scope of repurposed drugs. *Comput. Biol. Med.* 126, 104054.
- Skariyachan, S., Gopal, D., Muddebihalkar, A.G., Uttarkar, A., Niranjana, V., 2021. Structural insights on the interaction potential of natural leads against major protein targets of SARS-CoV-2: molecular modelling, docking and dynamic simulation studies. *Comput. Biol. Med.* 132, 104325.
- Srinivasan, S., Cui, H., Gao, Z., Liu, M., Lu, S., Mkandawire, W., Narykov, O., Sun, M., Korkin, D., 2020. Structural genomics of SARS-CoV-2 indicates evolutionary conserved functional regions of viral proteins. *Viruses* 12, 360.
- Starsich, F., Herrmann, I.K., Pratsinis, S.E., 2019. Nanoparticles for biomedicine: coagulation during synthesis and applications. *Annu. Rev. Chem. Biomol. Eng.* 10, 155–174.
- Tan, K.P., Varadarajan, R., Madhusudhan, M.S., 2011. DEPTH: a web server to compute depth and predict small-molecule binding cavities in proteins. *Nucleic Acids Res.* 39, W242–W248.
- Tang, Z., Zhang, X., Shu, Y., Guo, M., Zhang, H., Tao, W., 2021. Insights from nanotechnology in COVID-19 treatment. *Nano Today* 36, 101019. <https://doi.org/10.1016/j.nantod.2020.101019>.
- Tavakoli, S., Zahmatkeshan, M., Mohammadinejad, R., Mehrzadi, S., Joghataei, M.T., Alavijeh, M.S., Seifalian, A., 2021. The role of nanotechnology in current COVID-19 outbreak. *Heliyon*. 7, e06841 <https://doi.org/10.1016/j.heliyon.2021.e06841>.
- The UniProt Consortium, 2019. UniProt: a worldwide hub of protein knowledge. *Nucleic Acids Res.* 47, D506–D515.
- Trott, O., Olson, A.J., 2010. AutoDock Vina: improving the speed and accuracy of docking with a new scoring function, efficient optimization and multithreading. *J. Comput. Chem.* 31, 455–461.
- Ullrich, S., Nitsche, C., 2020. The SARS-CoV-2 main protease as drug target. *Bioorg. Med. Chem. Lett.* 30, 127377.
- Veber, F., Johnson, R., Chen, H.Y., Smith, B.R., Ward, K.W., Kopple, K.D., 2002. Molecular properties that influence the oral bioavailability of drug candidates. *J. Med. Chem.* 45, 2615–2623.
- Walls, A.C., Park, Y.J., Tortorici, M.A., Wall, A., McGuire, A.T., Veesler, D., 2020. Structure, function, and antigenicity of the SARS-CoV-2 spike glycoprotein. *Cell* 181, 281–292.e6.
- World Health Organization, 2020. Coronavirus Disease (COVID-19): Infection Prevention and Control. <https://covid19.who.int/> (Accessed 2021).
- World Health Organization, 2021. WHO Coronavirus (COVID-19) Dashboard. <https://covid19.who.int/table> (Accessed on 10 November 2021).
- Wrapp, D., Wang, N., Corbett, K.S., Goldsmith, J.A., Hsieh, C.L., Abiona, O., Graham, B. S., McLellan, J.S., 2020. Cryo-EM structure of the 2019-nCoV spike in the prefusion conformation. *Science* 367, 1260–1263.
- Yazdani, M., Glynn, L., Wright, L., Hawi, 1998. Correlating partitioning and Caco-2 cell permeability of structurally diverse small molecular weight compounds. *Pharma. Res.* 15, 1490–1494.
- Yin, W., Mao, C., Luan, X., Shen, D.D., Shen, Q., Su, H., Wang, X., Zhou, F., Zhao, W., Gao, M., Chang, S., Xie, Y.C., Tian, G., Jiang, H.W., Tao, S.C., Shen, J., Jiang, Y., Jiang, H., Xu, Y., Zhang, S., Zhang, Y., Xu, H.E., 2020. Structural basis for inhibition of the RNA-dependent RNA polymerase from SARS-CoV-2 by remdesivir. *Science* 368, 1499–1504.
- Yu, R., Chen, L., Lan, R., Shen, R., Li, P., 2020. Computational screening of antagonists against the SARS-CoV-2 (COVID-19) coronavirus by molecular docking. *Int. J. Antimicrob. Agents* 56, 106012.
- Yüce, M., Filiztekin, E., Özkaya, K.G., 2021. COVID-19 diagnosis -a review of current methods. *Biosens. Bioelectron.* 172, 112752.
- Zhang, L., Lin, D., Sun, X., Curth, U., Drosten, C., Sauerhering, L., Becker, S., Rox, K., Hilgenfeld, R., 2020. Crystal structure of SARS-CoV-2 main protease provides a basis for design of improved α -ketoamide inhibitors. *Science* 368, 409–412.
- Zhao, L., Chai, M.H., Yao, H.F., Huang, Y.P., Liu, Z.S., 2020. Molecularly imprinted polymers doped with carbon nanotube with aid of metal-organic gel for drug delivery systems. *Pharm. Res.* 37, 1–14.